

demonstrated over a large distance in the public fiber network of Greece [6]. This research opens promising directions for future technological applications.

On the other side, synchronization of chaotic lasers has fascinating fundamental aspects. The lasers are driven by time delayed couplings and feedback, and the system is well described by a set of ordinary difference-differential equations [7]. The delay terms generate high-dimensional chaos which is still a challenge to mathematical research [8]. In addition, various kinds of synchronization have been observed and analyzed for such chaotic systems, like complete, generalized, anticipated, lag and phase synchronization [9]. Spontaneous symmetry breaking and sub-lattice synchronization have recently been reported [10, 11].

Secret communication relies on the fact that an attacker (Eve) is not able to decode the message from the exchanged signal. If Eve does not know anything about the chaotic systems of Alice and Bob she still can try to analyze the exchanged signal using the tools of nonlinear dynamics [12]. If Eve, however, knows the chaotic equations used by Alice and Bob but not their secret parameters, Eve may try to estimate the parameters from the recorded signal.

If, in addition, Eve knows the parameters as well, then Eve knows everything which Alice and Bob know from each other. In this case one might guess that it is impossible to send secret messages. However, this is not true. Modern cryptographic methods generate a secret key over a public channel. These methods, which were pioneered by Diffie and Hellmann in 1976, are based on the number theory [13]. Recently, it has been suggested that public channel cryptography may be possible using synchronization of chaotic systems [14–16]. This novel promising aspect of nonlinear dynamics will be emphasized in this overview.

14.2 Synchronization of Chaotic Systems

Let us consider two dynamical systems x and y which are driven by a time-dependent signal s , as sketched in Fig. 14.1. These systems may be ordinary differential equation for high-dimensional variables $x(t)$ and $y(t)$,

$$\dot{x} = f(x, s), \quad \dot{y} = f(y, s) \quad (14.1)$$

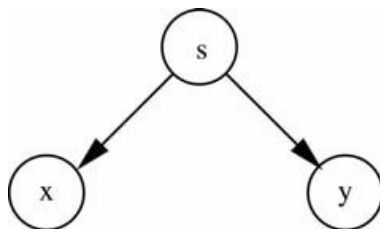


Fig. 14.1 A chaotic signal $s(t)$ drives two identical nonlinear systems x and y . The synchronous solution $x(t) = y(t)$ is stable if all conditional Lyapunov exponents are negative.

with some vector function f and some signal $s(t)$. For instructive simplicity we will demonstrate the principles of synchronization and communication with the simplest chaotic system, the iterated Bernoulli map [1, 9],

$$x_t = f(x_{t-1}), \quad f(x) = (ax) \bmod 1. \quad (14.2)$$

For $a > 1$ the trajectories x_t are chaotic with a flat density on the unit interval $[0, 1]$. In the following we consider $a > 1$, only. Using the Bernoulli map, the scenario of Fig. 14.1 may be realized as

$$\begin{aligned} x_t &= (1 - \varepsilon)f(x_{t-1}) + \varepsilon f(s_{t-1}) \\ y_t &= (1 - \varepsilon)f(y_{t-1}) + \varepsilon f(s_{t-1}). \end{aligned} \quad (14.3)$$

The parameter $\varepsilon \in [0, 1]$ controls the strength of the drive s . The sequence s_t may be generated from any mechanism like noise or an independent chaotic equation. Obviously, the synchronous trajectory $x_t^0 = y_t^0$ is a solution of Eq. (14.3). However, this solution may be unstable to tiny perturbations. Hence we consider small deviations from the synchronous state,

$$\delta x_t = x_t - x_t^0, \quad \delta y_t = y_t - y_t^0. \quad (14.4)$$

Expanding Eq. (14.3) yields

$$\delta x_t = (1 - \varepsilon)a \delta x_{t-1}, \quad \delta y_t = (1 - \varepsilon)a \delta y_{t-1}. \quad (14.5)$$

These equations show that the synchronous solution is stable if the Lyapunov exponent λ of the subsystem is negative,

$$(1 - \varepsilon)a < 1 \quad \text{or} \quad \lambda = \ln |(1 - \varepsilon)a| < 0. \quad (14.6)$$

Switching off the drive, the subsystems must not be chaotic, otherwise the synchronous trajectory is unstable [9].

Note that in this simple model the driving signal s_t does not appear in the stability analysis, since the derivative $f'(x_{t-1}^0) = a$ does not depend on the trajectory x_t^0 .

Pecora and Carroll [2] realized that the drive s may be a part of the chaotic system x , as indicated in Fig. 14.2. The left side represents the transmitter of Alice who sends the signal s to the receiver Bob. Bob is using s as a part of his dynamic equations, which are identical to those of Alice. Again we demonstrate this principle with the Bernoulli iteration:

$$\begin{aligned} s_t &= (1 - \varepsilon)f(s_{t-1}) + \varepsilon f(x_{t-1}), \\ x_t &= (1 - \varepsilon)f(x_{t-1}) + \varepsilon f(s_{t-1}), \\ y_t &= (1 - \varepsilon)f(y_{t-1}) + \varepsilon f(s_{t-1}). \end{aligned} \quad (14.7)$$

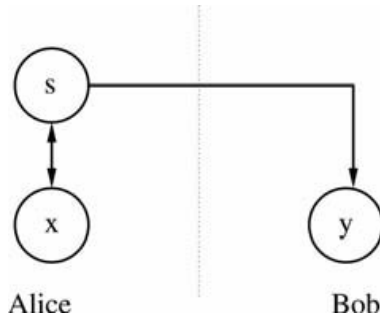


Fig. 14.2 The chaotic system of Alice is decomposed into a signal variable $s(t)$ and several passive variables $x(t)$. The signal $s(t)$ synchronizes the passive variables $y(t)$ of the identical nonlinear system of Bob.

The dynamics of Alice is chaotic since the stability matrix of the (s, x) system,

$$\begin{pmatrix} (1-\varepsilon)a & \varepsilon a \\ \varepsilon a & (1-\varepsilon)a \end{pmatrix} \quad (14.8)$$

always gives one positive Lyapunov exponent $\lambda = \ln a > 0$, independent of the strength ε of the drive. However, the stability of the synchronous solution $x_t = y_t$ is determined, as before, by Eq. (14.6). The total dynamic system of Alice is chaotic but the subsystems x and y are synchronous provided the conditional Lyapunov exponents are negative.

This is a general result which holds for iterated maps as well as for any chaotic system. Alice has to decouple her dynamic system into active and passive variables s and x . The active variables are inserted into the system of Bob. Bob's system can synchronize to Alice's provided the conditional Lyapunov exponents of the passive variables are negative.

To apply this scenario to communication one would like to send a scalar signal s which is part of a high-dimensional phase space (s, x) . Can a scalar signal synchronize high-dimensional chaos? The answer is positive. On the synchronization manifold $x_t = y_t$ there may exist a spectrum of positive Lyapunov exponents whereas perpendicular to this manifold any perturbation will relax back to the manifold, i.e., all conditional Lyapunov exponents are negative. This has been shown for Lorenz and Rössler equations and coupled map lattices [17]. In addition, this holds for dynamical systems with delay [8].

As mentioned before, the synchronization mechanism of Fig. 14.2 can be implemented by ordinary differential equations for $x(t), y(t)$ and $s(t)$. Such equations have been realized with electronic circuits of nonlinear elements [3, 18, 19]. Another fascinating possibility to realize communication by synchronization of chaotic systems are lasers. Applying a feedback to the laser cavity by injecting another beam – either from the laser itself or from another laser – the laser can be driven to a state of chaotic modulation of its intensity and phase [5, 8, 20, 21]. The time the light wave needs to go from Alice to Bob usually exceeds the time scales which determine the dynamics of a laser. Therefore, the two chaotic

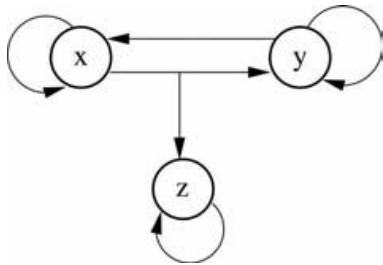


Fig. 14.3 Two dynamical systems x and y with delayed feedback are interacting by mutual delayed signals. An eavesdropper with an identical dynamical system z is driven by the signal from x , but cannot interact with the two partners.

systems of Alice and Bob are coupled by a time delayed signal with a delay time τ . This delay time just shifts the chaotic trajectories $y(t) = x(t - \tau)$. However, if additional delay times enter by self-feedback and if there is a bidirectional coupling between the lasers of Alice and Bob, the synchronization may become more complex, for example, anticipated chaos is possible [22].

Let us consider the configuration sketched in Fig. 14.3. Here three chaotic units are involved in the synchronization process: Alice and Bob are interacting by mutual coupling and Eve is driven by the signal of Alice. All three units have a self-feedback, and all exchanged signals – mutual, directed and self-feedback – are transmitted with an identical delay time τ . For simplicity, we again illustrate this mechanism with the Bernoulli map [1],

$$\begin{aligned} x_t &= (1 - \varepsilon)f(x_{t-1}) + \varepsilon\kappa f(x_{t-\tau}) + \varepsilon(1 - \kappa)f(y_{t-\tau}), \\ y_t &= (1 - \varepsilon)f(y_{t-1}) + \varepsilon\kappa f(y_{t-\tau}) + \varepsilon(1 - \kappa)f(x_{t-\tau}), \\ z_t &= (1 - \varepsilon)f(z_{t-1}) + \varepsilon\kappa f(z_{t-\tau}) + \varepsilon(1 - \kappa)f(x_{t-\tau}). \end{aligned} \quad (14.9)$$

Since feedback and exchange delay times are identical, the synchronous trajectory $x_t = y_t = z_t = x_t^0$ is a solution of these equations, with

$$x_t^0 = (1 - \varepsilon)f(x_{t-1}^0) + \varepsilon f(x_{t-\tau}^0). \quad (14.10)$$

The spectrum of Lyapunov exponents can be calculated exactly, using the method developed in [23]. In particular, in the limit of infinitely large delay times, $\tau \rightarrow \infty$, the equations have been solved analytically [11]. Here we consider this limit, only. For $\varepsilon > 0$ the system is in a state of high dimensional chaos, the Kaplan-Yorke dimension increases proportional to the delay time τ . For $\kappa = 0.5$ the two systems x and y receive an identical feedback, which in the limit of large delay time may be considered as noise. Hence, according to Eq. (14.6), x and y are synchronal for $\varepsilon > (a - 1)/a$.

If the two delay terms have different strength, $\kappa \neq 0.5$, the synchronal trajectory is stable for

$$\frac{a-1}{2a\varepsilon} < \kappa < \frac{2a\varepsilon - a + 1}{2a\varepsilon}, \quad \varepsilon > (a-1)/a. \quad (14.11)$$

Eve is not interacting with Alice and Bob. We assume that she is recording only the signal of Alice. Therefore, the area of stable synchronization is different from the one of Alice and Bob. If $x_t = y_t$ one finds for Eve

$$\kappa < \frac{a(\varepsilon - 1) + 1}{a\varepsilon}, \quad \varepsilon > (a-1)/a. \quad (14.12)$$

The phase diagram is shown in Fig. 14.4. There is no overlap between the range of parameters where Alice and Bob synchronize and where Eve is able to follow the trajectories of Alice and Bob. In particular, if in addition the exchanged signals are nonlinear functions of x_t and y_t , respectively, then Eve cannot adjust her parameters to synchronize with Alice and Bob.

This phenomenon is not specific to these simple maps, but it has also been found in corresponding experiments on chaotic semiconductor lasers [16]. Feedback with delay generates high-dimensional chaos which can be synchronized by exchanged laser beams. The experimental and corresponding numerical phase diagrams show different areas of synchronization between mutually coupled and directionally coupled lasers. If the self-feedback is absent, $\kappa = 0$ in Fig. 14.4, the iterated maps are not synchronized. For the semiconductor lasers, however, a symmetry breaking has been reported for this case: One laser takes the role of a leader which drives the opposite laser which follows with the delay time τ [10]. Since the time-shifted trajectories are not a solution of the corresponding Eqs. (14.9), the laser intensities do not completely coincide, they have a large overlap only.

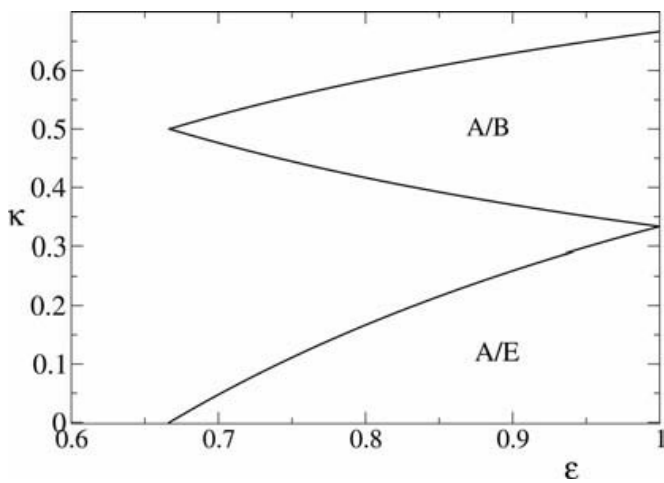


Fig. 14.4 Phase diagram of configuration of Fig. 14.3 where the three systems are Bernoulli maps with parameter $a = 3$ and infinite delay times. ε is the strength of the total time-delayed couplings, and $\kappa\varepsilon$ is the

strength of the self-feedback. In the upper region the two partners x and y synchronize, whereas only in the lower region the eavesdropper z can synchronize with y .

Note, however, in the case where Eve is recording both of the signals from Alice as well as Bob, she is able to synchronize her system. In this case one needs an asymmetry between self- and mutual feedback to prevent Eve from adjusting her parameters.

Two-way is different from one-way, interaction is more than drive, this principle promises novel methods of public channel cryptography which are explained in Sections 14.6–14.8. In the following section we will discuss how to encode a message $m(t)$ into the exchanged signal $s(t)$.

14.3

Coding and Decoding Secret Messages in Chaotic Signals

In the previous section we have seen that two systems which are in a state of high-dimensional chaos can be synchronized by a scalar signal $s(t)$ being exchanged between the two systems. For communication, a master/slave configuration is usually considered: Alice is transmitting a signal $s(t)$ to Bob which synchronizes his chaotic equations. Now Alice wants to use this mechanism to send a secret message to Bob. How can she encode the message $m(t)$ into the transmitted signal $s(t)$ such that an eavesdropper Eve recording the signal is not able to extract the message from the signal?

There are two ways to encode and decode a message into the chaotic system of Alice and Bob: 1. to modulate the transmitted signal $s(t)$ by the message $m(t)$, and 2. to modulate the dynamics of Alice's system $x(t)$ by the message. The first method is often called *chaos masking* while the second method has the names *chaos modulation* or *chaos shift keying*.

Let us demonstrate these two principles with the Bernoulli maps. In the simplest case of Fig. 14.1 the two systems x_t and y_t are driven by an external random signal s_t . Now Alice is sending an additional signal $\tilde{s}_t = x_t + m_t$ to Bob. Since Bob is synchronal to Alice, he just can subtract his own variable from this signal to recover the message,

$$m_t = \tilde{s}_t - y_t. \quad (14.13)$$

If the dynamics is complex enough, and if the message has a small amplitude compared to the carrier x_t , then it is not easy to extract the message from the transmitted signal s_t without knowing the dynamical equations of Alice and Bob.

In this simple example of chaos masking, however, one has to transmit two signals s_t and \tilde{s}_t . But it is possible to transmit a secret message by a single scalar signal s_t , only. In the simplest case, the message is just added to one of the internal variables, $s_t = x_t + m_t$. Now there are two possibilities, illustrated in Fig. 14.5: The signal influences the dynamics of the transmitter (chaos modulation, left side) or the signal is immediately transmitted to the receiver (chaos masking, right). In the first case, it is possible, in principle, to decode the mes-

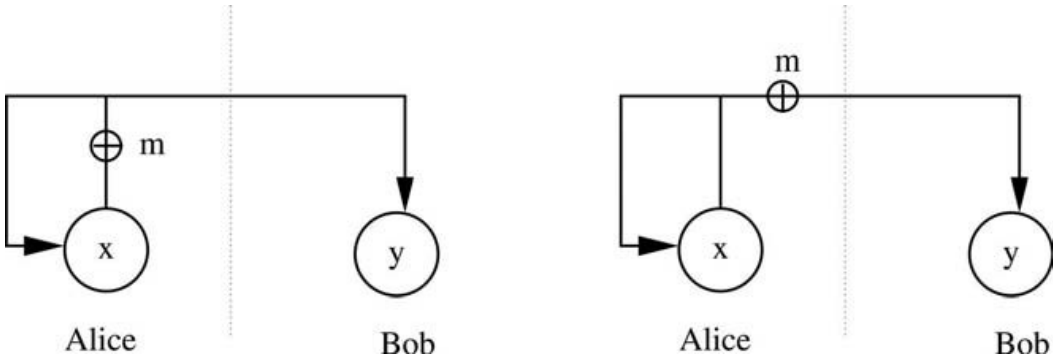


Fig. 14.5 Encoding a secret message m . Left: Chaos modulation. The message modulates the dynamics of Alice's equations, and Bob can extract the message without errors. Right: Chaos masking. The message is added to the exchanged signal and extracted by the mechanism of chaos pass filter.

age without any error. In the second case, decoding relies on a phenomenon which has been named *chaos-pass filter* [20]. Let us illustrate these two cases with the iterated maps with delay. The equations for chaos modulation are

$$\begin{aligned} s_t &= x_t + m_t, \\ x_t &= (1 - \varepsilon)f(x_{t-1}) + \varepsilon f(s_{t-\tau}), \\ y_t &= (1 - \varepsilon)f(y_{t-1}) + \varepsilon f(s_{t-\tau}). \end{aligned} \quad (14.14)$$

The dynamics of the receiver y_t is identical to the one of the transmitter x_t , thus the system synchronizes, $x_t = y_t$, if the subsystem has negative Lyapunov exponents, i.e., for $\varepsilon > (a - 1)/a$ [11]. The receiver is recording the transmitted signal s_t , hence he can immediately decode the message, $m_t = s_t - y_t$.

For the other case, the equations for chaos masking are

$$\begin{aligned} s_t &= x_t + m_t, \\ x_t &= (1 - \varepsilon)f(x_{t-1}) + \varepsilon f(x_{t-\tau}), \\ y_t &= (1 - \varepsilon)f(y_{t-1}) + \varepsilon f(s_{t-\tau}). \end{aligned} \quad (14.15)$$

The receiver has a different dynamics than the transmitter, thus they do not synchronize perfectly. However, they still have a large overlap with each other and the message can also be decoded with the difference $m_t = s_t - y_t$. But there is an error, the recovered message has only some overlap to the original one.

It is not obvious why chaos masking is working. The dynamical system y_t is driven by the sum $x_t + m_t$. Nevertheless, it follows a trajectory which is close to the dynamics of the transmitter, $x_t \simeq y_t$. The chaotic system filters the message out of the drive. It functions as a *chaos-pass filter*. This phenomenon is not well understood, yet, although it seems reasonable that perturbations perpendicular to a stable synchronization manifold are damped [24].

Both of the encoding/decoding methods, chaos modulation as well as chaos-pass filter, have been implemented in electronic circuits as well as in chaotic lasers [3, 5, 19, 25, 26]. In most cases a directed coupling – a master/slave configuration – has been used. Only recently, a chaos-pass filter has applied to mutual couplings in the context of public key cryptography [16]. This method will be introduced in Section 14.8.

There are other possibilities to encode a message into a chaotic system. For instance, the parameters of the transmitter can be modulated with the message. In particular, if the message is binary, $m_t \in \{0, 1\}$, the receiver may be synchronal for $m_t = 0$ and detuned for $m_t = 1$. If one of the transmitter variables is transmitted, then the receiver knows whether the corresponding variable of his dynamical system can follow ($m_t = 0$) or not ($m_t = 1$). For chaotic lasers, these parameters which are modulated by the message may be the pump current or the phase shift. Modulating the phase shift corresponds to modulating the delay time τ [25].

14.4

Analysis of the Exchanged Signal

The secret message which Alice sends to Bob is encoded in a chaotic signal on the transmission line. An eavesdropper Eve is recording this signal. If Eve does not know the dynamics which generates the signal, is she still able to recover the message from the transmitted signal?

In fact, nonlinear dynamics offers many powerful tools to analyze data produced by deterministic chaos [12]. Chaotic trajectories of dissipative system usually move on low-dimensional manifolds which may be reconstructed from partial information on the trajectories. Accordingly, from the transmitted signal $s(t)$ a low-dimensional manifold can be constructed, and an additional encoded message may be extracted from deviations from this manifold.

Consequently, for the early implementations of chaos-based communication by Lorenz equations, the encoded message was extracted by the technique of return maps [27]. The maxima and minima of the transmitted signal were recorded and consecutive differences and sums of these data were plotted. This return map clearly showed almost one-dimensional segments. A message encoded either by chaos modulation or by chaos masking generated points away from these segments. Hence this message could easily be extracted, at least for low frequencies. For high frequencies, however, the message could be directly reconstructed from the power spectrum of the transmitted signal.

Chaotic lasers offer additional structures which can be used to extract messages by the technique of return maps. The output intensity of chaotic lasers consists of a series of irregularly spaced pulses. The sequence of intensity maxima and time intervals of these spikes was plotted as return maps. The relation between intensity maxima and interspike intervals allowed to extract a message encoded in the transmitted laser beam [28].

14.5

Neural Cryptography

In the previous sections, we have seen how secret messages can be encoded in a chaotic system. Alice and Bob have to use an identical dynamical system with identical parameters. If an attacker Eve knows these equations as well as their parameters she should be able to extract the message, too.

However, this is only true for directed couplings. In this case Alice and Bob have to use a secure private channel to agree on a common encryption key, namely the secret parameters of their equations. In the following sections we show how Alice and Bob can send secret messages over a public channel without previous agreements over secure private channels. Eve knows all the details about the system, equations, parameters as well as any exchanged information; nevertheless she is not able to decode the secret message which Alice is transmitting to Bob.

The first dynamical system which was developed for public key exchange is based on the synchronization of artificial neural networks which are trained on their mutual outputs [14]. This method has been named neural cryptography. It consists of a simple algorithm for discrete variables which can easily be implemented on small integrated circuits. And it allows new kinds of cryptographic protocols, since the algorithm is continuously generating new encryption keys. From the point of nonlinear dynamics, neural cryptography may be considered as an ensemble of random walks with reflecting boundaries which is synchronized by public chaotic (random) signals. This random walk is controlled by binary signals transmitted between the two partners over the public channel [34].

For neural cryptography, each partner has a multilayer neural network, a tree parity machine, as shown in Fig. 14.6. Each network consists of KN input units $x_{k,i}$, K hidden units σ_k and one output unit τ . There is a layer of synaptic weights $w_{k,i}$ between the input and hidden units. These weights are discrete variables with a depth L ,

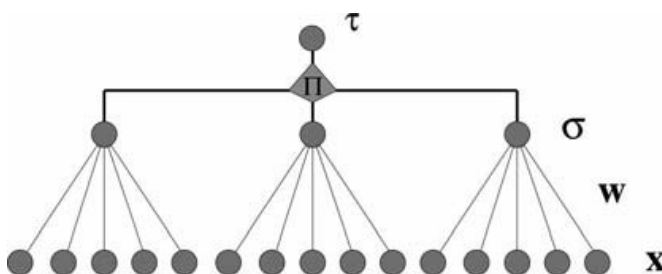


Fig. 14.6 Multilayer neural network (tree parity machine) used for neural cryptography. x_k : Public random input vectors. w_k : Synaptic weights with discrete components. σ : Hidden units. τ : Output bit, the product

of the hidden units. Alice and Bob are transmitting their output bits and train their synaptic weights according to the configuration of their hidden units.

$$w_{k,i} \in \{-L, -L+1, \dots, L-1, L\}, \quad k = 1, 2, \dots, K; \quad i = 1, \dots, N. \quad (14.16)$$

Typical values of these parameters are $K = 3, L = 3, N = 1000$. Given $K = 3$ input vectors \mathbf{x}_k , the hidden units and the output of the network are calculated from

$$\sigma_k = \text{sign}(\mathbf{w}_k \cdot \mathbf{x}_k), \quad \tau = \sigma_1 \sigma_2 \sigma_3. \quad (14.17)$$

Hence the value of a hidden unit is just the sign of the vector product of the corresponding N -dimensional input and weight vectors. The output bit of the network is given by the product of the hidden units.

The dynamics of the two networks of Alice and Bob is defined by the following algorithm: At each time step K new common random input vectors \mathbf{x}_k are generated. Alice and Bob calculate their hidden units and output units. If the two output bits are different, they start with a new common input vector. If the two output bits are identical, $\tau^A = \tau^B$, they change their synaptic weights in the direction of the input vectors, but only for these hidden units, which agree with the two output bits.

Each component of the weight vectors \mathbf{w}_k is driven by the corresponding component of the input vector \mathbf{x}_k . Since Alice and Bob are driven by the same input vectors, their components are performing almost identical random walks and synchronize due to the reflecting boundaries. The updates of the components are controlled by the internal state of the system; the output and hidden units are functioning like on/off signals. This leads to attractive as well as repulsive steps for the weight vectors of Alice and Bob, and the synchronization process is a competition between these two kinds of steps. Finally Alice and Bob synchronize completely, and the common synchronized weight vectors perform an identical random walk in the KN -dimensional hypercube.

The generation of the secret key is defined as follows: Alice and Bob are starting from private random weight vectors \mathbf{w}_k^A and \mathbf{w}_k^B , respectively. At each time step they receive K public input vectors \mathbf{x}_k , exchange their output bits τ^A and τ^B and update their synaptic weights. As soon as they are synchronized, they use their identical synaptic weights as a common secret key. This secret key may either be used for standard encryption networks, or Alice and Bob continue the dynamics without exchanging bits but using them as one-time pad for encryption.

An eavesdropper Eve knows all the details of the algorithm and records all the transmitted bits. She knows the sequence of input vectors, as well. Hence she uses an identical neural network and trains it using the same rules. However, there is an important difference: Alice and Bob are reacting to their mutual output bits, they are interacting. Eve, on the other hand, can only listen to the communication, but she cannot interact. It turns out that Alice and Bob have a higher probability for attractive steps than Eve [35]. That leads to a short synchronization time for Alice and Bob while Eve needs a very long time to synchronize [40]. Since the dynamics is stopped when Alice and Bob have identical weight vectors, the probability of a successful attack of Eve is very low.

In the limit of large keys, $N \rightarrow \infty$, scaling laws could be derived, which quantitatively define the level of security of neural cryptography [14, 34]. It turns out that the synaptic depth L , i.e., the number of possible states of each component $w_{k,i}$ of the weight vectors, is the essential parameter which controls the security. The probability of a successful attack of Eve decays exponentially with L

$$P_E \propto e^{-\gamma L}. \quad (14.18)$$

Increasing the value of L increases the synchronization time t_{syn} of Alice and Bob. But this time increases only polynomially with L ,

$$t_{\text{syn}} \propto L^2. \quad (14.19)$$

Consequently, the security of neural cryptography can be increased to any desired level without increasing the effort for synchronization too much.

Of course, there may exist many extensions of this method to improve either the security or the success of attacks. The security could be improved by combining neural networks with chaotic maps or by selecting appropriate input vectors (queries). The eavesdropper could make use of an ensemble of networks in genetic or majority attacks. But after all these investigations, the scaling laws, Eqs. (14.18) and (14.19), could be recovered. Neural cryptography appears to be secure.

Recently, this method has been implemented in integrated circuits [36]. It promises novel cryptographic protocols and applications.

14.6

Public Key Exchange by Mutual Synchronization

Neural cryptography, discussed in Section 14.5, has shown that it is possible to generate a secret key over a public channel key by a stochastic process. An eavesdropper Eve may know all the details of the communication process, nevertheless Eve is not able to synchronize with Alice and Bob and extract the secret message from the transmitted signals. In neural cryptography, the random or chaotic drive is generated by an external mechanism. In this section, we report on investigations to extend the idea of public key exchange to mutual synchronization to chaotic differential equations without an external drive [37].

Each of the two partners Alice and Bob is using a set of Lorenz equations with identical public parameters in the chaotic regime. The two Lorenz systems are coupled by a function $s(t)$ of their variables. The equation of Alice is, for example,

$$\begin{aligned}\frac{dx^A}{dt} &= 10(y^A - x^A) + K[s^B(t) - s^A(t)], \\ \frac{dy^A}{dt} &= 28x^A - y^A - x^A z^A, \\ \frac{dz^A}{dt} &= x^A y^A - \frac{8}{3}z^A.\end{aligned}\tag{14.20}$$

Bob has the identical equations for his variables, and since Eve knows these equations she will use corresponding equations for her variables, too. The signals $s^A(t)$ and $s^B(t)$ are transmitted between Alice and Bob, and Eve is recording them.

The main problem is to find signals $s^A(t), s^B(t)$, which first synchronize Alice with Bob, second, do not synchronize Eve with Alice, and third, do not allow to extract the variables of Alice using the tools of nonlinear dynamics discussed in Section 14.4. Given such signals, Alice and Bob can use some digits of their synchronized variables $x^A(t)$ and $x^B(t)$ for a secret key.

To meet the conditions 1 and 2, [37] suggests to take a nonlinear function $s(t)$ of the variable $x(t)$ with two time delays,

$$s^A(t) = x^A(t - \tau_1) + \text{sign}(x^A(t - \tau_1)) A (x^A(t - \tau_1) - x^A(t - \tau_2))^2.\tag{14.21}$$

It turns out that the coupling values K , where Alice and Bob synchronize but Eve does not, are limited to an interval, only. Figure 14.7 shows the largest con-

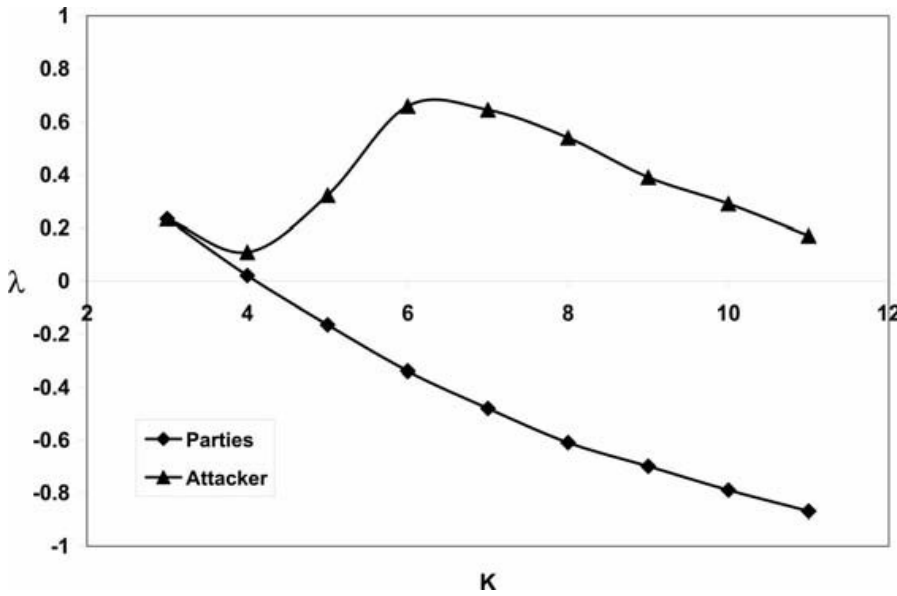


Fig. 14.7 Largest conditional Lyapunov exponents of three Lorenz systems coupled by nonlinear time-delayed signals with strength K . The lower curve is the result for the two partners interacting by mutual signals while the upper curve is the result for an eavesdropper using the signal of one partner.

ditional Lyapunov exponent of the A/B and A/E systems. Only for Alice and Bob there is a range of negative exponents. For large values of K the systems diverge. Hence, even if Eve tries to adjust her parameter K she will not be able to synchronize with Alice and Bob.

Subsequent calculations, however, have shown that the function of Eq. (14.21) can be analyzed with the tools of Section 14.4. The variable $x(t)$ can be estimated by embedding $s(t)$ in a three-dimensional phase space. But the function $s(t)$ of Eq. (14.21) can be extended such that the tools of nonlinear dynamics do not work, at least with a feasible computational effort. In [37] the amplitude A of Eq. (14.21) was replaced by a nonlinear function of $s^A(t)$ and $s^B(t)$ and a common public noise was added. Embedding techniques were not successful for those signals.

Although the system of Eve does not synchronize with the ones of Alice and Bob, its trajectory may stay in the vicinity of the synchronization manifold. Hence one has to consider – as in neural cryptography – the probability that Eve recovers the first α digits of the variable $x^A(t)$. Figure 14.8 shows that this success probability decreases exponentially with the number α , whereas the synchronization time increase linear with α . The security of the method is even stronger if Alice, Bob, and Eve are using a ring of N Lorenz equations instead of a single Lorenz triplet. The ring has internal couplings as well as mutual ones as in Eq. (14.21). Numerical simulations showed that the success probability decreases exponentially with the number N of Lorenz triplets, whereas the

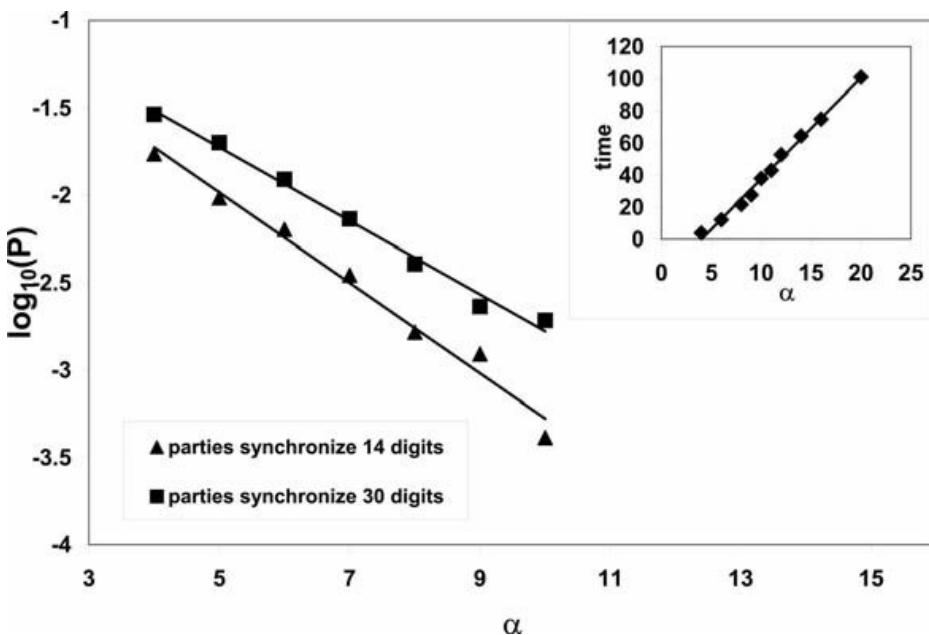


Fig. 14.8 Probability that an eavesdropper can extract the first α digits of the key variable x^A , after the two partners have synchronized their key variables to 14 or 30 digits, respectively.
Inset: Synchronization time of the partners as a function of precision α .

synchronization time increases linearly with N , only. Similar to neural cryptography, public key exchange by chaos synchronization can be adjusted to any level of security.

14.7

Public Keys by Asymmetric Attractors

In the two previous sections, the methods of nonlinear dynamics have been used to construct a public key exchange protocol. A secret key could be generated between two partners although the exchange of the information as well as any details of the algorithm are known to any attacker who is recording the communication between the two partners.

The two previous methods were based on complete synchronization of two chaotic systems. Consequently, both partners used identical dynamical systems; these key exchange protocols were symmetric. Asymmetric protocols, on the other hand, may offer some advantages with respect to security and authorization. Thus it is interesting to look for asymmetric encryption protocols based on nonlinear dynamics.

Such an asymmetric method has been suggested by Tenny et al. [15]. The transmitter T and the receiver R are using different dynamical systems. The one of the transmitter is public whereas the receiver uses a private system which is unknown to the transmitter and any eavesdropper. Both sides are sending signals $s_T(t)$ and $s_R(t)$ which drive the whole dynamical system.

The message $m(t)$ is included into the signal $s_T(t)$ sent by the transmitter T. Let us consider the case where the message consists of bits, $m = 0, 1$. The system of the transmitter depends on the value of $m(t)$. The complete system, transmitter as well as receiver, has two attractors, one for $m = 0$ and one for $m = 1$. Since the receiver knows the complete dynamical system he can simulate it for $m = 0$ as well as for $m = 1$, and he finally can decide to which of the two attractors the exchanged signal $s_T(t)$ comes closest. Hence the receiver recovers the transmitted bit m with some error rate which depends on the mutual overlap between the two attractors.

An eavesdropper may record the two signals $s_T(t)$ and $s_R(t)$. But she does not know the dynamical system of R. Thus she cannot simulate the complete system and cannot determine the two attractors for $m = 0$ and $m = 1$. Of course, if the process is repeated many times, the eavesdropper can distinguish between two attractors, using the embedding methods for $s_T(t)$ of the tool box of nonlinear dynamics [12]. Consequently, the receiver has to use a new dynamical system for each single received bit.

Similar to the methods of the two previous sections, this algorithm is based on mutual interaction: The transmitter is sending the message encoded into its dynamical variables while the receiver drives the systems of the transmitter by some of his own variables. In principle, this method opens the possibility to construct asymmetric public encryption protocols based on nonlinear dynamics.

In practice, its first version is still inconvenient since the dynamics has to be changed after each bit, and its security against advanced attacks has still to be investigated.

14.8

Mutual Chaos Pass Filter

In Section 14.2 we have seen that a bidirectional coupling may lead to synchronization whereas, using identical parameters, a system driven by only one of the partners does not synchronize. If, however, the driven system receives the signals from both of the two partners it is not so easy to prevent synchronization of the eavesdropper. But also in this case bidirectional coupling is different from unidirectional one, and one may try to use this difference for secure communication.

In fact, recently a mechanism has been suggested which has the potential of secure public channel communication. This mechanism was named *mutual chaos-pass filter* [16]. It allows the two partners to transmit bits on top of a chaotic signal with a very low bit error rate. The transmission is bidirectional, both partners are sending secret messages to each other. An eavesdropper recording the bidirectional chaotic signal can recover the messages only with a high bit error rate. The difference of bit error rates between the partners and the attacker can be amplified using repetition codes, and finally a secure communication can be realized by transmission of compressed blocks of bits of suitable lengths. Consequently, a quantitative difference of bit error rates between partners and for the attacker is sufficient to realize a secure public channel communication.

Let us demonstrate the principle of mutual chaos-pass filter with chaotic maps as in Section 14.2. The only difference to Fig. 14.3 and Eq. (14.9) is that now Alice is adding a message m_t and Bob is adding noise n_t to their transmitted signals. Hence Eq. (14.9) has to be extended to

$$s_t^x = x_t + m_t, \quad s_t^y = y_t + n_t. \quad (14.22)$$

$$A : x_t = (1 - \varepsilon)f(x_{t-1}) + \varepsilon\kappa f(x_{t-\tau}) + \varepsilon(1 - \kappa)f(s_{t-\tau}^y). \quad (14.23)$$

$$B : y_t = (1 - \varepsilon)f(y_{t-1}) + \varepsilon\kappa f(y_{t-\tau}) + \varepsilon(1 - \kappa)f(s_{t-\tau}^x). \quad (14.24)$$

$$E : z_t = (1 - \varepsilon)f(z_{t-1}) + \varepsilon\kappa f(s_{t-\tau}^y) + \varepsilon(1 - \kappa)f(s_{t-\tau}^x). \quad (14.25)$$

In the following we show results for the logistic map $f(x) = |4x(1 - x)|$, for a binary message $m_t \in \pm m$ and for a uniform distribution of noise $n_t \in [-r, r]$. The system of Bob is driven by the signal $x_t + m_t$, he is responding with y_t and sending $y_t + n_t$. It turns out that Bob's response is almost identical to the state of x_t of Alice, thus Bob can recover the message from

$$m_t^B = \text{sign}(s_t^x - y_t). \quad (14.26)$$

30

Control of Synchronization in Oscillatory Neural Networks

Peter A. Tass, Christian Hauptmann, and Oleksandr V. Popovych

30.1

Introduction

Synchronization is a generic phenomenon of interacting oscillators, which has been observed and studied in many fields in physics, engineering, chemistry, biology, and medicine (see e.g. [27, 39, 54, 73, 76, 99]). Synchronization processes are of crucial importance for brain function. Well-coordinated synchrony within and between neuronal populations appears to be an important mechanism for neuronal signaling and information processing [69, 73]. In contrast, pathologically strong synchronization processes may severely impair brain function as, e.g., by Parkinson's disease (PD), essential tremor, or epilepsy [15, 16, 34, 63, 92]. Parkinsonian resting tremor, for instance, appears to be caused by a population of neurons located in the thalamus and the basal ganglia. These neurons fire in a synchronized and intrinsically periodical manner at a frequency similar to that of the tremor, regardless of any feedback signals [41, 43, 52]. In contrast, under physiological conditions, these neurons fire incoherently [51]. In patients with PD this neuronal cluster acts like a pacemaker and activates premotor areas and the motor cortex [2, 96], where the latter synchronize their oscillatory activity [89] and drive muscles causing the peripheral shaking.

In patients with medically refractory movements disorders, e.g., with advanced PD or essential tremor, depth electrodes are chronically implanted in target areas like the thalamic ventralis intermedius nucleus or the subthalamic nucleus [4, 6]. Electrical deep brain stimulation (DBS) is performed by administering a permanent high-frequency (HF) (> 100 Hz) periodic pulse train via the depth electrodes [4, 6]. HF DBS has been developed empirically and its mechanism is not yet fully understood [48]. It appears to strongly alter the neuronal firing and basically mimics the effect of tissue lesioning, e.g., by suppressing neuronal firing, which, in turn, suppresses the peripheral tremor [48, 95]. HF DBS is reversible and has a much lower rate of side effects than lesioning with thermocoagulation [68]. However, HF DBS may lead to side effects like dysarthria, dysesthesia, and cerebellar ataxia [95]. On the other hand, 11–15% of PD

patients have unsatisfactory outcomes concerning tremor suppression in spite of proper electrode placement [19, 42].

To improve deep brain stimulation novel stimulation techniques have been developed with methods from statistical physics and nonlinear dynamics (see [76] and references below). The goal of these techniques is to selectively counteract the pathological synchronization processes. We here present three methods which are particularly effective and robust against parameter variations and, hence, promising for therapeutic applications:

- (i) *Multisite coordinated reset stimulation* (Section 30.2) [84, 85]: Brief and mild resetting stimuli are administered at different sites at subsequent times and cause an effective transient desynchronization. Desynchronized firing is maintained by repetitive administration of multisite coordinated reset stimuli.
- (ii) *Linear multisite delayed feedback stimulation* (Section 30.3) [29–31]: The activity of a neuronal population is permanently registered, amplified, and fed back at different sites with different delays. By its tendency to split the whole population into entrained and phase shifted sub-populations, the multisite echo counterbalances the population's tendency to synchronize in phase, so that a robust desynchronization is achieved.
- (iii) *Nonlinear delayed feedback stimulation* (Section 30.4) [57–59]: The activity of a neuronal population is permanently registered and fed back after nonlinear processing. The perturbation caused by this distorted echo causes a powerful desynchronization at minimal and practically vanishing stimulation currents. This method specifically counteracts the pathological interactions, so that the neurons' natural frequencies get restored.

A novel, theoretically fascinating and clinically highly relevant aspect emerges, if we take into account synaptic plasticity, i.e., the fact that the nervous system adapts the strength of the neurons' synaptic interaction (coupling) to the timing of the neurons' firing. As shown theoretically [32, 88, 90, 91], networks with synaptic plasticity may unlearn their tendency to produce synchronized activity. Desynchronizing stimulation may reshape the connectivity (coupling) pattern and induce long-lasting effects. This approach may lead to powerful and even curative stimulation techniques (see Section 30.5).

30.2

Multisite Coordinated Reset Stimulation

Based on Winfree's pioneering phase resetting studies of circadian rhythms [98], the effects of a pulsatile stimulus on the amplitude and, in particular, the phase dynamics of a single oscillator were analyzed in detail [23, 98, 99]. With topological methods Winfree showed that an oscillation can be annihilated by a stimulus of a critical intensity and duration administered at a critical initial phase [98, 99]. The phase resetting approach has been used to investigate the reactions of a single neuron to a pulsatile electrical stimulus; both theoretically [5] and experimentally [26].

Neuronal synchronization processes are of crucial importance under physiological [69] as well as pathological [15, 16, 34, 63, 92] conditions. Furthermore, noise is inevitable in biological systems [22]. To understand brain functioning and to design effective therapeutic stimulation techniques, which work in the presence of noise, it is necessary to understand stimulation induced synchronization and desynchronization of neuronal populations. For this reason stochastic phase resetting has been studied in both ensembles of uncoupled oscillators [74, 75] and ensembles of coupled oscillators [76] subject to noise. This leads to effectively desynchronizing stimulation techniques, such as double pulse stimulation [77, 78, 82], stimulation with a brief high-frequency pulse train followed by a single pulse [79], and stimulation with a brief low-frequency pulse train followed by a single pulse [80, 81]. These methods share one particular feature: each stimulus consists of two qualitatively different stimuli. The first stimulus is stronger and resets (restarts) the ensemble, whereas the second, weaker stimulus is a single pulse which is administered after a constant time delay and desynchronizes by hitting the cluster in a vulnerable state. All of these methods require a precise calibration of the stimulus parameters.

In contrast, multisite coordinated reset stimulation does not require any time-consuming calibration [84, 85]. This method causes an effective desynchronization and is particularly robust against parameter variations, e.g., variations of the neurons' mean frequency. Multisite coordinated reset stimulation means that a synchronized population of neurons is stimulated with a sequence of brief resetting stimuli (typically brief high-frequency stimulus trains) via different sites. The delay between the subsequent resetting stimuli equals τ/n , where $\tau \approx T$, T is the mean period of the synchronized oscillation, and n is the number of stimulation sites [84, 85]. The subsequent reset of different sub-populations induces a so-called cluster state, i.e., the whole population splits into n sub-populations which differ with respect to their mean phase. From the cluster state the neurons typically relax to a uniformly desynchronized state before they revert back to the in-phase synchronized state, if left unperturbed. Hence, to maintain a desynchronized firing, multisite coordinated reset stimuli have to be administered repetitively. Multisite coordinated reset stimulation exploits transient responses which are due to the oscillators' (pathologically strong) interactions.

We model the neuronal population with a network of N phase oscillators [17, 25, 28, 39] and, in addition, take into account stimulation and random forces [76]:

$$\dot{\psi}_j = \Omega - \frac{K}{N} \sum_{k=1}^N \sin(\psi_j - \psi_k) + X_j(t) S_j(\psi_j) + F_j(t), \quad (30.1)$$

where ψ_j is the phase of the j th phase oscillator. All oscillators have the same eigenfrequency Ω and are globally coupled with strength $K > 0$. In neurons the impact of an electrical stimulus depends on the neuron's phase [5, 26]. Hence,

the stimulus is modeled by a 2π -periodic function like $S_j(\psi_j) = I \cos \psi_j$ with the intensity parameter I . Stimulus administration is modeled by

$$X_j(t) = \begin{cases} 1 & \text{neuron } j \text{ is stimulated at time } t \\ 0 & \text{else} \end{cases}. \quad (30.2)$$

The random forces $F_j(t)$ are Gaussian white noise with $\langle F_j(t) \rangle = 0$ and $\langle F_j(t) F_k(t') \rangle = D \delta_{jk} \delta(t - t')$, where D is a constant noise amplitude. For vanishing stimulation ($X=0$), Eq. (30.1) is the well-known Kuramoto model of coupled phase oscillators [39].

A phase-dependent stimulus, like $S_j(\psi_j) = I \cos(\psi_j)$ resets the j th oscillator to a particular phase provided the intensity parameter I is large compared to the coupling strength and to the noise amplitude and provided the stimulation duration is long enough [76, 83]. Such a reset can be achieved with a strong single pulse [76, 78, 82, 86], a HF pulse train (with a pulse rate 20 times larger than the mean eigenfrequency Ω) [79] or a low-frequency pulse train (with a pulse rate similar to Ω) [80, 81]. We here use a HF pulse train for the reset.

Let us, first, assume that there is no noise ($D=0$). A HF pulse train with $S_j(\psi_j) = I_j \cos(\psi_j + \theta)$ resets the j th neuron close to the phase $\psi_j^{\text{res}} + \theta$ [76, 83]. Hence, we could easily desynchronize the population by stimulating each neuron separately to achieve equidistant resets. For this, we would administer HF pulse trains of identical timing (i.e., $X_j(t) = X(t)$ for $j=1, \dots, N$) but different stimulation mechanisms $S_j(\psi_j) = I_j \cos[\psi_j + 2\pi(j-1)/N]$. After such a phase-scattering stimulation the population would be perfectly desynchronized, with a uniform distribution of the phases $\psi_j^{\text{res}} + 2\pi(j-1)/N$. However, stimulating each neuron separately would require the use of many electrodes and would easily damage or even destroy the neural tissue. Furthermore, noise makes the reset less perfect. Therefore, we choose a different approach. Instead of inducing a perfectly uniform distribution of the phases, we simply split the population into a few, say four, sub-populations which are equally spaced in a cycle $[0, 2\pi]$.

We denote as *sub-population 1, 2, 3, and 4* the groups of neurons $j=1, \dots, N/4$, $j=N/4+1, \dots, N/2$, $j=N/2+1, \dots, 3N/4$, and $j=3N/4+1, \dots, N$, respectively (with N divisible by 4). To split the population in four equally spaced sub-populations we may choose qualitatively different strategies: (i) *Simultaneous stimulation* of all four sub-populations: Phase shifts of the reset neurons are induced by phase shifts of the stimulation mechanisms. We stimulate neuron j of sub-population $k=1, \dots, 4$ with a HF pulse train with $S_j(\psi_j) = I \cos[\psi_j + 2\pi(k-1)/4]$. (ii) The four sub-populations are *stimulated at different times with identical stimulation mechanisms* S_j . The delay between subsequent HF pulse trains is equal to $T/4$, where $T=2\pi/\Omega$ is the period of the population without stimulation. We may stimulate neuron j of sub-population $k=1, \dots, 4$ at time $t' + T(k-1)/4$ with a HF pulse train with $S_j(\psi_j) = I \cos(\psi_j)$. (iii) Strategies (i) and (ii) can be combined, e.g., by performing *two subsequent antiphase resets of pairs of sub-populations with a time delay of $T/4$* (Fig. 30.1(a)). Sub-population 1 and 2 are stimulated simultaneously at time t' , but with different polarity. A neuron of sub-population 1 is stimulated with

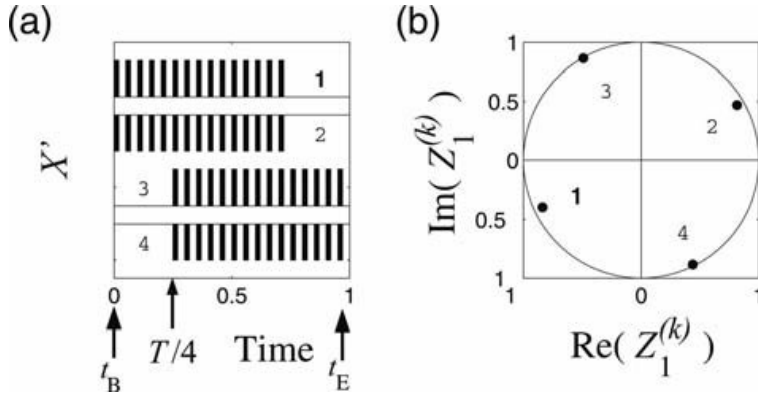


Fig. 30.1 (a) Two subsequent antiphase resets of pairs of sub-populations are achieved by administering two pairs of high-frequency (HF) pulse trains with different polarity with a time delay of $T/4$, where $T = 2\pi/\Omega$ is the period of the population. Time course and polarity of HF pulse trains is schematically indicated with $X'(t) = X(t)S_j(0)$, where the numbers indicate the sub-population to which the corresponding HF pulse train is administered. Single pulses are highlighted by shaded regions. Each HF pulse train consists of 15 single pulses with duration of 0.02, intersected by pauses of length 0.03.

HF pulse trains 1 and 3 have positive polarity: $S_j(\psi_j) = I \cos(\psi_j)$, whereas HF pulse trains 2 and 4 have negative polarity: $S_j(\psi_j) = -I \cos(\psi_j)$, with $I = 30$. Stimulation starts at time $t_B = 0$ and ends at $t_E = 0.97$. (b) Stimulating model (30.1) according to (a) results in a configuration at the end of the stimulation given by $Z_1^{(k)}(t_E)$ where numbers indicate the corresponding sub-population $k = 1, \dots, 4$. The unit circle marks the maximal range of $|Z_1^{(k)}|$. Model parameters: $N = 100$, $K = 2$, $\Omega = 2\pi$, noise amplitude $D = 0.4$.

$S_j(\psi_j) = I \cos(\psi_j)$, whereas a neuron of sub-population 2 is stimulated with $S_j(\psi_j) = I \cos(\psi_j + \pi) = -I \cos(\psi_j)$. Analogously, sub-populations 3 and 4 are simultaneously stimulated at time $t' + T/4$. A neuron of sub-population 3 is stimulated with $S_j(\psi_j) = I \cos(\psi_j)$, whereas a neuron of sub-population 4 is stimulated with $S_j(\psi_j) = -I \cos(\psi_j)$.

Variant (i) requires that we are able to modify the stimulation mechanism $S(\psi_j)$ itself. This might be difficult in an experimental application. In contrast, variants (ii) and (iii) operate with identical pulses of the same or different polarity, administered at different times. Numerically variants (i)–(iii) work comparably well. We here consider version (iii). To estimate the extent and type of synchronization of the whole population we use the cluster variables

$$Z_m(t) = R_m(t)e^{i\varphi_m(t)} = \frac{1}{N} \sum_{j=1}^N e^{im\psi_j(t)}, \quad (30.3)$$

where $R_m(t)$ and $\varphi_m(t)$ are the corresponding real amplitude and real phase, where $0 \leq R_m(t) \leq 1$ for all times t [7, 76]. Cluster variables are convenient for characterizing synchronized states of different types: Perfect in-phase synchronization corresponds to $R_1 = 1$, whereas an incoherent state, with uniformly distributed phases, is associated with $R_m = 0$ ($m = 1, 2, 3, \dots$). $R_1 = 0$ combined with large R_m is indicative of an m -cluster state consisting of m distinct and equally

spaced clusters, where within each cluster all oscillators have similar phase. Analogously, we use

$$Z_m^{(k)}(t) = R_m^{(k)}(t) e^{i\varphi_m^{(k)}(t)} = \frac{4}{N} \sum_{j \in \Lambda_k} e^{im\psi_j(t)}, \quad (30.4)$$

as cluster variables for the four sub-populations separately. $k=1, \dots, 4$ is the index of the sub-population introduced above, m is the index referring to an m -cluster state (see Eq. (30.3)), and Λ_k is the set of indices belonging to the k th sub-population, e.g., $\Lambda_1 = \{1, \dots, N/4\}$. With $Z_1^{(k)}$ we estimate the extent of in-phase synchronization within sub-population k . The latter is perfectly in-phase synchronized if $R_1^{(k)} = 1$.

The effect of a multisite coordinated reset is illustrated with a snapshot of $Z_1^{(k)}(t_E)$, the centers of mass of all four sub-populations at the end of the stimulation (Fig. 30.1(b)). All four sub-populations are strongly synchronized, where their mean phases $\varphi_1^{(k)}$ are equally spaced in the cycle. $R_1^{(1)}$ and $R_1^{(2)}$ are a bit smaller than $R_1^{(3)}$ and $R_1^{(4)}$. This follows from the fact that at the end of the HF pulse trains 1 and 2 (i.e., at time $t_E - T/4$) $Z_1^{(1)}$ and $Z_1^{(2)}$ are located exactly where $Z_1^{(3)}$ and $Z_1^{(4)}$ are located at the end of the HF pulse trains 3 and 4 (i.e., at the end of the stimulation, at time t_E). Between $t_E - T/4$ and t_E sub-populations 1 and 2 spontaneously run in the counterclockwise direction through a quarter of a cycle and relax to a less synchronized state with smaller $R_1^{(1)}$ and $R_1^{(2)}$. The arrangement of $Z_1^{(1)}, \dots, Z_1^{(4)}$ at the end of the stimulation is a symmetrical 4-cluster state of the whole population, with R_4 from (30.3) close to 1 and R_1 close to 0. The coordinated reset splits the whole populations in four distinct, symmetrically arranged sub-populations.

To understand how a stimulus-induced clustering leads to an effective desynchronization, we study the dynamics of the leading modes Z_1, \dots, Z_4 . We first recall the dynamical behavior of model (30.1) without stimulation (with $X(t) = 0$ in (30.2)). For large N it has been shown that noisy in-phase synchronization emerges out of the incoherent state due to a decrease of the noise amplitude D or, analogously, because of an increase of the coupling strength [39, 76]. For $K > D$ a stable limit cycle $Z_1(t) = Y \exp(i\Omega t)$ emerges, where Y is a complex constant [76]. When K exceeds its critical value $K^{\text{crit}} = D$, Z_1 from (30.3) becomes an *order parameter*, which according to the slaving principle [27] governs the dynamics of the other, stable modes Z_m ($m = 2, 3, \dots$) on the center manifold [56]: The order parameter Z_1 acts on a slow time scale, whereas the stable modes Z_m act on a fast time scale and relax to values given by the order parameter Z_1 [27, 102]. In model (30.1) with large N this relationship reads [76]:

$$R_m \propto R_1^\nu \text{ with } \nu \geq 2, m = 2, 3, 4, \dots \quad (30.5)$$

The collective dynamics will not only be visualized with the cluster variables Z_m , but also by considering the collective firing. A single firing/bursting model neuron fires/bursts whenever its phase is close to zero (modulo 2) [17, 25, 28,

39, 76]. We illustrate the collective firing with the *relative number of neurons producing an action potential or burst* at time t given by

$$n_{\text{fire}}(t) = \frac{\text{number of neurons with } \cos \varphi_j > 0.99}{N}. \quad (30.6)$$

$0 \leq n_{\text{fire}}(t) \leq 1$ for all t . $n_{\text{fire}}(t) = 0$ means that no neuron fires/bursts, while all neurons fire/burst at time t if $n_{\text{fire}}(t) = 1$. Varying the threshold parameter 0.99 in a reasonable range does not change the results.

Figure 30.2 shows the dynamics before, during and after stimulation. The phase at which the coordinated reset from Fig. 30.1 is applied to the same neuronal population is varied within one cycle. The impact of this stimulus is independent of the phase at which it is administered. At the end of the stimulation the system has reached the 4 cluster-state shown in Fig. 30.1 (a): R_4 has a value similar to the prestimulus range, whereas R_1 , R_2 and R_3 are close to zero. In the poststimulus period the system does not remain in the 4 cluster-state.

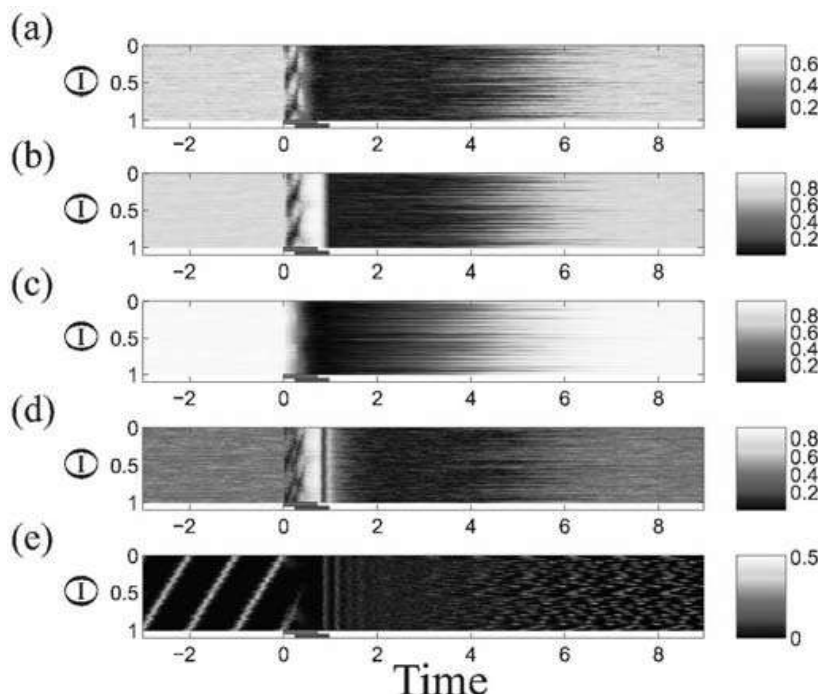


Fig. 30.2 The stimulus from Fig. 30.1 (a) is administered to the in-phase synchronized neuronal population from Eq. (30.1) at different initial phases. At the beginning of each simulation the phases are given by $\psi_j = \Psi + \Delta\psi_j$, where $\Delta\psi_j$ is normally distributed with variance $\sqrt{0.3}$. The time course of R_1 (a), R_2 (b), R_3 (c), R_4 (d) from Eq. (30.3), and the relative number of firing neurons n_{fire} from Eq. (30.6) (e) is shown in 101 simulations, where the normalized mean ini-

tial phase $\Theta = \Psi/2\pi$ is varied in equidistant steps within one cycle $[0, 1]$. The first 30 periods were discarded to guarantee that the stimuli hit the population in a stable synchronized state. Same stimulation parameters and model parameters as in Fig. 30.1. Stimulation starts at $t_B = 0$ and ends at $t_E = 0.97$. Pairs of HF pulse trains 1, 2 and 3, 4 are indicated by green and blue horizontal bars, respectively.

Rather due to the slaving principle R_4 rapidly decays to zero, so that the system approaches a perfectly desynchronized state characterized by $R_m = 0$ ($m = 1, 2, 3, 4, \dots$). The vanishing R_1 suppresses R_4 according to (30.5). Without coupling (but with noise) the 4 cluster-state would decay more slowly (see [74]). From the mathematician's viewpoint the relaxation of R_4 is due to the system being attracted by the center manifold as characterized by (30.5). By imposing a 4 cluster-state, the stimulation does only half of the desynchronizing work. The rest, namely approaching a uniformly desynchronized state, is done by the system itself. In this way the coupling, which causes the synchronization, is used for improving the desynchronizing effect.

In the course of the poststimulus transient R_1 and according to (30.5) also R_2 , R_3 , and R_4 recover again. The system finally reaches its stable in-phase synchronized state again.

In summary, by shifting the system into an unstable 4-cluster state, the system reacts by automatically running through a desynchronized state. Finally, the system reverts back to the synchronized state, if left unperturbed. The results are stable with respect to variations of N between 20 and 1000 and more.

The effectively desynchronizing multisite coordinated reset can be used to block the resynchronization. For this, we may use three different control strategies:

(i) *Periodic administration of coordinated reset stimuli*: The most simple, open loop type of stimulation is a periodic administration of coordinated reset stimuli.

(ii) *Demand-controlled timing of the administration of identical stimuli*: Whenever the population tends to resynchronize, the same stimulus is administered (Fig. 30.3). The larger the coupling strength K , the more often a stimulus has to be administered to maintain an uncorrelated firing. In an experimental application one has to observe the synchronized oscillation during a sufficiently long period of time in order to perform a frequency analysis which yields the period T of the population in the absence of stimulation and, thus, the critical stimulation parameter $T/4$ (the time delay between the two pairs of HF pulse trains, see Fig. 30.1(a)).

(iii) *Entrainment with periodically administered HF pulse trains of demand-controlled length*: The stimuli are periodically administered with offset times $t_n = n v \tau$, where $n = 0, 1, 2, 3, \dots$ is the index labeling different stimuli, $\tau = T + \varepsilon$ is a time interval in the range of the period T of the population without stimulation, and v is a small integer such as 2 or 3. This means we perform a $1:v$ entrainment of the four sub-populations, where the spontaneous frequency of the neurons is approx. v times larger compared to the frequency of stimulus administration. The smaller $|\varepsilon|$, the smaller is the stimulation strength necessary to achieve an entrainment.

The closed-loop variants (ii) and (iii) require that the ensembles activity can be measured appropriately. Unlike in Fig. 30.1(a), we use HF pulse trains of demand-controlled length: The length of the HF pulse trains increases linearly between a minimal value M_{\min} and a maximal value M_{\max} of single pulses (except

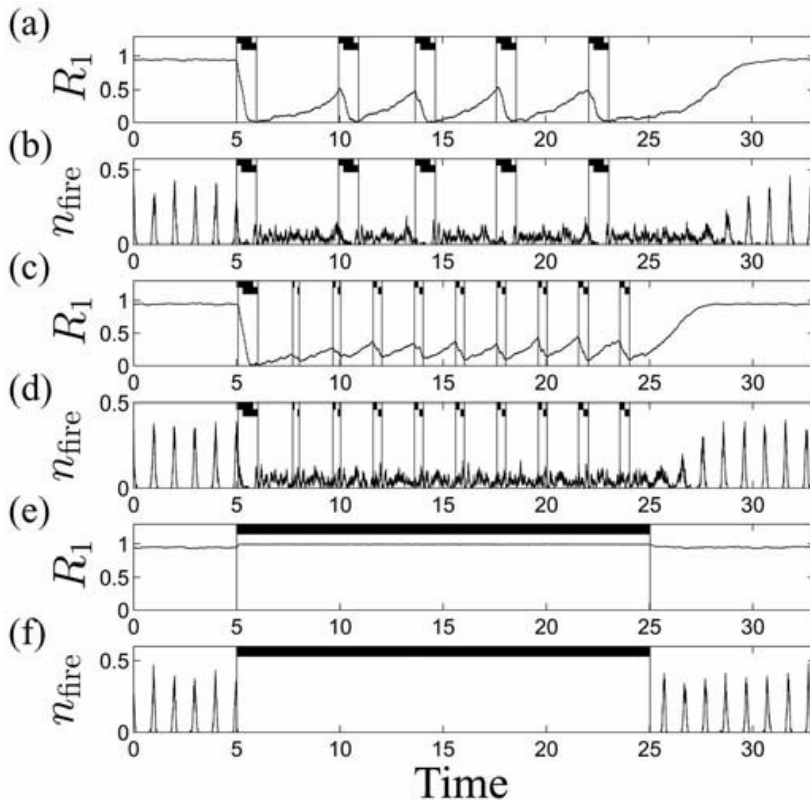


Fig. 30.3 Time course of R_1 from Eq. (30.3) (a), (c), and (e)) and of n_{fire} from Eq. (30.6) (b), (d), (f) during different types of stimulation. *Demand-controlled timing of stimulus administration* (a) and (b): As soon as the amplitude R_1 of the recovering order parameter reaches the value of 0.5, the stimulus from Fig. 30.1 (a) is administered again. *Periodical stimulation with demand-controlled length of HF pulse train* (c) and (d): The stimulus from Fig. 30.1 (a) is administered periodically, where the length of the HF pulse trains is adapted to R_1 according to Eq. (30.7) with

$M_{\max} = 15$ and $M_{\min} = 0$. *Standard permanent HF pulse train stimulation* (e) and (f): Each neuron is stimulated with the same HF pulse train: $X_j(t) = X(t)$ in Eqs. (30.1) and (30.2). (a)–(f): Numerical integration, model parameters, and initial conditions as in Fig. 30.2. Begin and end of stimuli are indicated by vertical lines. (a)–(d): Upper and lower shaded regions correspond to pairs of HF pulse trains 1, 2 and 3, 4, respectively. (e) and (f): HF pulse train is indicated by one.

for rounding), where the latter is initially used for desynchronizing the fully synchronized population. R_1 is measured at times $t'_n = t_n - t_{\max}$, where t_{\max} is the maximal duration of a HF pulse train (containing M_{\max} single pulses). $R_1(t'_n)$ determines the number of pulses of the HF pulse trains 1–4 of the n th stimulus according to

$$M_n = \min \left\{ \left[\frac{R_1(t'_n)(M_{\max} - M_{\min})}{R_1(t_0)} \right]_{\mathbb{Z}} + M_{\min}, M_{\max} \right\}, \quad (30.7)$$

where $n = 0, 1, 2, 3, \dots$, $[x]_{\mathbb{Z}}$ stands for rounding x to the nearest integer, and $\min \{x_1, x_2\}$ stands for the minimum of $\{x_1, x_2\}$. The n th stimulus ends precisely at time $t_n = n\tau$, whereas it starts somewhere between t'_n (for $M_n = M_{\max}$)

and t_n (for $M_n = M_{\min} = 0$), depending on its duration. With this adaptive entrainment we stabilize the periodic motion of $Z_1^{(1)}, \dots, Z_1^{(4)}$, the centers of mass of the four sub-populations. In this way only minor corrections are necessary to keep the centers of mass $Z_1^{(1)}, \dots, Z_1^{(4)}$ sufficiently close to their corresponding attractors (Fig. 30.1(b)) at times $t_n = n\tau$. If the suppression of R_1 is not sufficient we may (i) choose a larger intensity parameter I in $S_j(\psi_j) = I \cos \psi_j$, (ii) increase M_{\min} , (iii) administer the stimuli at a higher rate, i.e., decrease ν , so that the inter-stimulus interval $t_{n+1} - t_n = \tau$ gets smaller, and/or (iv) increase the duration of each single pulse of the pulse trains. The feedback value of R_1 can also be evaluated before time t'_n , especially in case of a slow order parameter dynamics (i.e., when the coupling is weak with respect to the noise). We could also use the mean of R_1 in a period of evaluation.

Applying the standard, permanent HF pulse train stimulation [4, 6] to our model (30.1) (in a first approximation) corresponds to stimulating each neuron with the same HF pulse train [$X_j(t) = X(t)$ in (30.1), (30.2)]. During a permanent HF stimulation a high-frequency entrainment of the order parameter Z_1 captures Z_1 in a small portion of the Gaussian plane [79], so that the individual neurons' firing is stopped, but no desynchronization occurs (Fig. 30.3(e) and (f)). In contrast, during stimulation R_1 is larger compared to its prestimulus level, and after stimulation the synchronous firing continues immediately. To suppress the firing with such a simple pulse train persistently, it has to be administered permanently. The number of single pulses used to suppress the firing in Fig. 30.3(e) and (f) is 5.35 and 8.02 times larger than that used for blocking the resynchronization in Fig. 30.3(a) and (b) and (c), (d), respectively. This illustrates the effectiveness of the demand-controlled multisite coordinated reset stimulation. The latter can effectively desynchronize stimulated oscillators with a significantly smaller amount of stimulation current compared to the standard permanent HF pulse-train stimulation.

30.3

Linear Multisite Delayed Feedback

In this section we present another technique for effective and robust desynchronization of neuronal populations. As in the previous section, the presented desynchronization technique is also based on the stimulation of a strongly synchronized population of interacting oscillators. The stimulation is administered via several sites, e.g., four sites, where through each stimulation site an individual stimulation signal is applied. The individual stimulation signals are derived from the delayed mean field of the ensemble. Therefore, the macroscopic activity (mean field) of the controlled population is measured, delayed, amplified and fed back in a spatially coordinated way via the stimulation sites using different delays for each stimulation site, respectively [29–31]. More precisely, let the stimulation electrodes be E_n , $n = 1, 2, 3, 4$, where the individual stimulation signals S_n are administered via the electrodes E_n , respectively. We denote the mea-

chronizing multisite coordinated reset stimulation presented through four equally distributed electrodes, results in a reduction of the synaptic connectivities which, finally, ends up in a stabilization of the desynchronized state which outlasts the epoch of desynchronizing stimulation (see Fig. 30.10(c)). If the mean synaptic connectivity is analyzed separately for the cluster of functionally related neurons (MC_5), i.e., the five neurons which receive the additional external input, and for the neurons not affected by the additional input (MC_{95}), Fig. 30.10(d) illustrates that kindling stimulation disturbs the cluster of functionally related neurons while multisite coordinated reset stimulation leaves this cluster unperturbed, in particular the connectivities of the functionally related neurons are able to recover during the desynchronizing stimulation (Fig. 30.10(d) and (e)).

Therapeutically rewiring stimuli of this kind [32, 88, 90, 91] shift the population into the basin of attraction of the stable desynchronized state in an extremely mild way leaving clusters of functionally related neurons unperturbed. This concept might contribute to a novel therapeutic stimulation strategy for the therapy of neurological and psychiatric diseases characterized by abnormal synchrony [21]. Instead of suppressing pathological synchronization this approach aims at reshaping neural networks in a way that they unlearn their tendency to generate pathological synchrony. According to our theoretical results [32, 88, 90, 91] this requires considerably less stimulation current as compared to standard high-frequency stimulation. Also Fig. 30.10 illustrates why we do not expect that maladaptive processes, i.e., the formation of misconnected clusters, occur. Desynchronizing stimulation specifically counteracts pathological synchrony in this way giving rise to the reemergence of physiological patterns of connectivity.

30.6

Discussion

In this chapter we presented three methods for the control of collective dynamics in ensembles of interacting oscillators. These methods are coordinated reset stimulation (Section 30.2), linear multisite delayed feedback (Section 30.3), and nonlinear delayed feedback (Section 30.4). We have shown that all three methods can effectively suppress the undesirable synchronization among oscillators, where the latter continue to exhibit their natural oscillatory activity. In contrast, high-frequency pulse train stimulation of sufficient strength blocks the individual oscillators.

The coordinated reset stimulation requires repetitive (demand-controlled or simple periodic) stimulus administration, where the stimulated oscillators are kept in a permanent transient between synchronized and desynchronized states. With such a stimulation protocol, the amount of the administered stimulation current is significantly smaller than that of the high-frequency stimulation. This allows us to expect much less side effects because of the smaller current spread

when this technique is being used for the deep brain stimulation. Multisite coordinated reset stimulation also works in simulations with realistic stimulation and interaction topologies [84, 85]. Unlike other stimulation techniques, which are based on phase resetting principles and require thorough calibration [77–82], multisite coordinated reset stimulation distinguishes itself by the absence of critical stimulation parameters, by the robustness of the desynchronizing effect, and by the quick availability (without time consuming calibration).

Linear multisite delayed feedback allows to control cluster-states in the stimulated system. On the one hand, depending on the chosen stimulation parameter τ , one can induce an N -cluster state, where N refers to the number of electrodes used for the stimulation. On the other hand, linear multisite delayed feedback stimulation provides an effective method for the control of spatiotemporal dynamics. Applied to CPGs, which are neural networks that can endogenously (i.e., without external drive) produce oscillatory patterned outputs [3, 11, 14, 45, 97], i.e., anatomically distinct, but interacting clusters of neurons, our approach might induce a coordinated sequential firing of different clusters. Different arrangements of the delays can cause different types of dynamics which might control different locomotor patterns. In this way, linear multisite delayed feedback stimulation maintains spatially patterned synchrony with minimal amounts of stimulation. Hence, linear multisite delayed feedback stimulation might be tested for the restoration of CPG activity in patients with incomplete spinal cord injury [11, 12] or gait ignition disorders [66].

By stimulation with *nonlinear delayed feedback*, the synchronization of the stimulated oscillators can effectively be enhanced, if the coupling strength and stimulus amplification are weak. On the other hand, for any coupling strength, even for very strong coupling, the synchronization can be effectively suppressed, if the stimulus amplification parameter is large enough, which is the main feature of the nonlinear delayed feedback. In the latter case, the stimulation restores the natural frequencies of the oscillators suppressed by synchronization. We approximate the decay rate of the order parameter of the stimulated ensemble and the amplitude of the stimulation signal, which characterize the extent of synchrony among the oscillators and the amount of the administered stimulation force, respectively. Both quantities decay with increasing stimulus amplification according to the power law (30.14). This scaling is extremely important for medical applications. Translated into the context of electrical brain stimulation, Eq. (30.14) means that the better the pathological synchrony is suppressed, the less stimulation current is needed. The stimulation can lead to a multistability of stimulation-induced desynchronized states, where the mean frequency of the stimulated ensemble can significantly be detuned by stimulation. This may open up a novel avenue for the frequency control of ensembles of interacting oscillators, for example, for populations of oscillatory neurons in the brain. We note that the discussed method demonstrates a great robustness with respect to system and stimulation parameter variations, which is of primary importance for applications. The NDF method also demonstrates a broad applicability and universality, which has been tested on a number of coupled networks of differ-

ent nature including ensembles of synaptically coupled bursting neurons and for a variety of stimulation protocols (see [57–59, 87]).

Desynchronizing stimulation might effectively counteract pathological neuronal synchronization processes, in order to achieve an effective suppression of symptoms. Moreover, desynchronizing stimulation might even reshape affected neuronal networks, to induce long-lasting therapeutic effects (see Section 30.5). This approach might, hence, lead to a fundamentally novel therapy for diseases characterized by pathological brain synchrony.

References

- 1 L.F. Abbott and S.B. Nelson. Synaptic plasticity: taming the beast. *Nat. Neurosci.*, 3:1178–1183, 2000.
- 2 W.W. Alberts, E.J. Wright, and B. Feinstein. Cortical potentials and parkinsonian tremor. *Nature*, 221:670–672, 1969.
- 3 M.C. Bellingham. Driving respiration: the respiratory central pattern generator. *Clin. Exp Pharmacol Physiol.*, 25:847–856, 1998.
- 4 A.L. Benabid, P. Pollak, C. Gervason, D. Hoffmann, D.M. Gao, M. Hommel, J.E. Perret, and J. de Rougemont. Longterm suppression of tremor by chronic stimulation of ventral intermediate thalamic nucleus. *The Lancet*, 337:403–406, 1991.
- 5 E.N. Best. Null space in the Hodgkin-Huxley equations: a critical test. *Biophys. J.*, 27:87–104, 1979.
- 6 S. Blond, D. Caparros-Lefebvre, F. Parker, R. Assaker, H. Petit, J.-D. Guieu, and J.-L. Christiaens. Control of tremor and involuntary movement disorders by chronic stereotactic stimulation of the ventral intermediate thalamic nucleus. *J. Neurosurg.*, 77:62–68, 1992.
- 7 H. Daido. Order function and macroscopic mutual entrainment in uniformly coupled limit-cycle oscillators. *Prog. Theor. Phys.*, 88:1213–1218, 1992.
- 8 H. Daido. Order function theory of macroscopic phase-locking in globally and weakly coupled limit-cycle oscillators. *Int. J. Bif. Chaos*, 7(4):807–829, 1997.
- 9 D. Debanne, B.H. Gahweiler, and S.M. Thompson. Long-term synaptic plasticity between pairs of individual CA3 pyramidal cells in rat hippocampus slice cultures. *J. Physiol.*, 507:237–247, 1998.
- 10 A. Destexhe, M. Rudolph, J.M. Fellous, and T.J. Sejnowski. Fluctuating synaptic conductances recreate in-vivo-like activity in neocortical neurons. *Neuroscience*, 107:13–24, 2001.
- 11 V. Dietz. Spinal cord pattern generators for locomotion. *Clinical Neurophysiol.*, 114:1379–1389, 2003.
- 12 V. Dietz and R. Müller. Degradation of neuronal function following a spinal cord injury: mechanisms and countermeasures. *Brain*, 127:2221–2231, 2004.
- 13 K. Dolan, A. Witt, M.L. Spano, A. Neiman, and F. Moss. Surrogates for finding unstable periodic orbits in noisy data sets. *Phys. Rev. E*, 59:5235–5241, 1999.
- 14 J. Duysens and H.W. van de Crommert. Neural control of locomotion; the central pattern generator from cats to humans. *Gait Posture*, 7(2):131–141, 1998.
- 15 R.J. Elble and W.C. Koller. *Tremor*. John Hopkins University Press, Baltimore, 1990.
- 16 J. Engel and T.A. Pedley. *Epilepsy: A Comprehensive Textbook*. Lippincott-Raven, Philadelphia, 1997.
- 17 B. Ermentrout and N. Kopell. Multiple pulse interactions and averaging in systems of coupled neural assemblies. *J. Math. Biol.*, 29:195–217, 1991.
- 18 U. Ernst, K. Pawelzik, and T. Geisel. Delay-induced multistable synchronization of biological oscillators. *Phys. Rev. E*, 57:2150–2162, 1998.
- 19 M.C. Rodriguez-Oroz et al. Bilateral deep brain stimulation in Parkinson's disease: a multicentre study with 4 years follow-up. *Brain*, 128(10):2240–2249, 2005.

31

Control of Cardiac Electrical Nonlinear Dynamics

Trine Krogh-Madsen, Peter N. Jordan, and David J. Christini

31.1

Introduction

The heart is a very complex and highly nonlinear system. Its predominant role is to function as a mechanical pump for the circulatory system. To do so, at each heart beat, the cells of the heart are stimulated by a typical propagation sequence of electrical activity. Disruption of this electrical pattern may lead to cardiac arrhythmias.

Despite the complexity of the heart, its electrical behavior can be studied using a variety of experimental and clinical techniques, and can be modeled mathematically using relatively simple systems of nonlinear differential equations. While these approaches have in recent years allowed great headway into understanding the dynamical behavior of the heart, cardiac arrhythmias such as ventricular fibrillation still claim the lives of hundreds of thousands of people each year in the United States alone [1]. Bridging the gap between understanding the mechanistic bases of arrhythmias and applying such knowledge to improve therapy presents one of the greatest challenges in the field of cardiac electrophysiology.

This chapter describes recent progress in attempting to control certain cardiac arrhythmias. In Sections 31.2 and 31.3 we give an introduction to cardiac electrophysiology and cardiac arrhythmias. A discussion on current therapies and their limitations is presented in Section 31.4. In Section 31.5, we describe recent advances toward controlling a certain type of abnormal heart rhythm called electrical alternans, which may act as a precursor for more complex and potentially lethal arrhythmias. Finally, in Section 31.6, we present recent progress in control of these more complex arrhythmias themselves. It is worth noting that chapter 32 by S. Sinha and S. Sridhar (“Controlling Spatiotemporal Chaos and Spiral Turbulence in Excitable Media”) in this volume deals more specifically with control of cardiac fibrillation.

31.2

Cardiac Electrophysiology

Efficient pumping of blood throughout the body requires that the heart musculature contracts in a coordinated manner. Given that the contraction of individual myocytes is driven by electrical excitation (through a process known as excitation–contraction coupling [7]), coordinated cardiac contraction requires that different regions of the heart be electrically activated in a specific sequence. This sequential activation is facilitated by the anatomical arrangement of the heart into distinct but contiguous regions whose electrophysiological properties are markedly different [53]. Figure 31.1 illustrates the normal conduction system. A normal sequence is initiated in the natural pacemaker of the heart (the so-called sinoatrial (SA) node) when the transmembrane voltage of cells transiently increases, then decreases, over a time course of a few hundred milliseconds. This voltage change is known as an action potential. Because the SA nodal region is electrically coupled to the right atrium, activation of the SA node causes a wave of activation to spread throughout the atria. Electrical activation of the atria is soon followed by mechanical contraction of the atria.

Electrical excitation of the atria leads to activation of the atrioventricular (AV) node, the anatomical location of which is indicated in Fig. 31.1. In anatomically

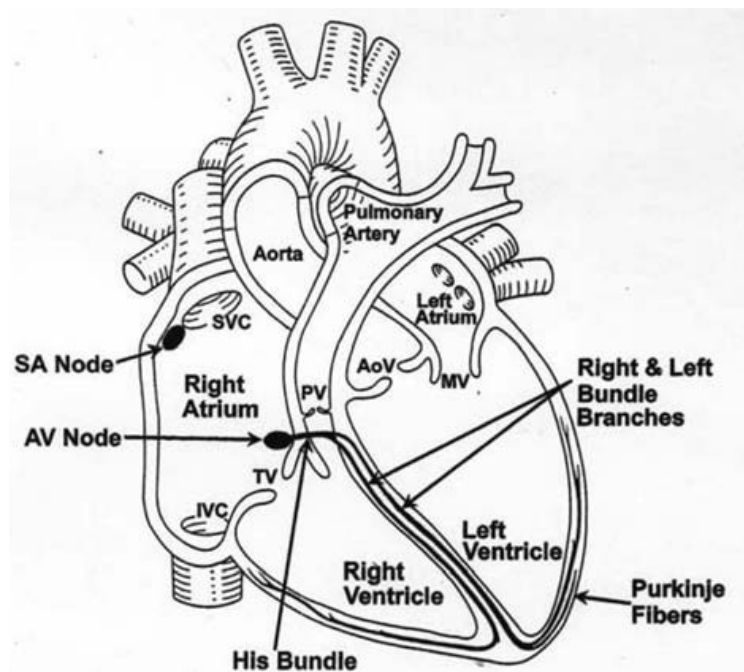


Fig. 31.1 A schematic diagram of the anatomical layout of the heart. The diagram illustrates a number of the major electrophysiological components of the heart, including the SA and AV nodes and the His-Purkinje system. PV: pulmonary vein, MV: mitral valve, TV: tricuspid valve, AoV: aortic valve, SVC: superior vena cava, IVC: inferior vena cava (reproduced from [40] with permission).

normal hearts, the AV node provides the only electrical connection between the atria and ventricles. The activation of the AV node leads to the subsequent excitation of the bundle of His, the left and right bundle branches, and the Purkinje fibers. Branches of the His-Purkinje system radiate throughout the ventricular tissue, and thus excitation of the His-Purkinje system leads to the excitation and subsequent contraction of the ventricles. The electrophysiological properties and anatomical layout of the AV node and His-Purkinje conduction system ensure that sufficient time exists for blood to flow from the atria to the ventricles before the ventricles contract. Ventricular contraction forcefully propels oxygenated blood from the left ventricle into the aorta and the systemic circulation, and deoxygenated blood from the right ventricle into the pulmonary artery and the pulmonary circulation (Fig. 31.1).

31.2.1

Restitution and Alternans

At the cellular level, the action potential is generated by the diffusion of ions through specialized channels in the cell membrane. The conductance of the membrane to the various ions present in the body varies as the channels open and close. This opening and closing generally depends nonlinearly on transmembrane potential and on time. One consequence of this is the phenomenon of restitution. Restitution is generally quantified by the restitution curve, which is a functional representation of the duration of an action potential (APD) versus the preceding rest period (the diastolic interval, or DI). An example is shown in Fig. 31.2. Such a curve reduces the high-dimensional dynamics of the cardiac cell to a simple one-dimensional approximation, expressed mathematically as the discrete map equation $APD_{n+1} = f(DI_n)$.

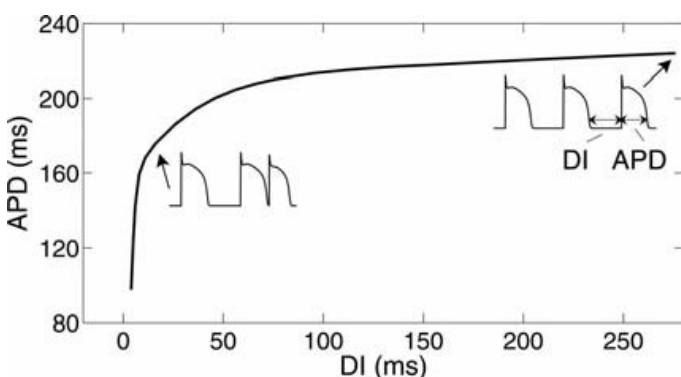


Fig. 31.2 A typical action potential duration (APD) restitution curve, generated with the Shiferaw et al. model [54] of a ventricular cell. To generate the APD restitution curve, a train of action potentials are stimulated at a constant pacing rate, followed by one premature stimulus. Thus, the diastolic interval

(DI) following the penultimate action potential is varied, and the duration of the resulting action potential is plotted as a function of the preceding DI. As the action potentials in the insets demonstrate, APD shortens as DI is shortened, leading to a restitution curve with the general shape as shown.

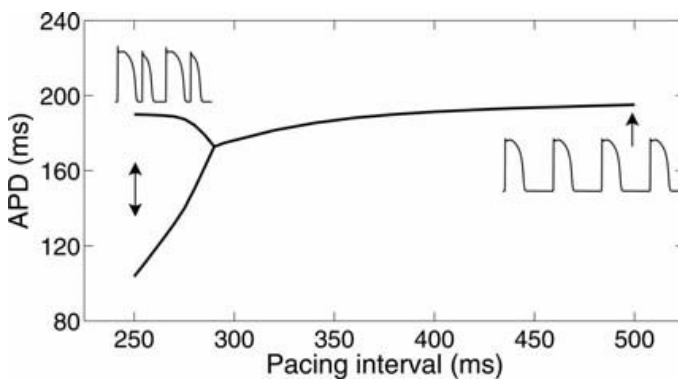


Fig. 31.3 Action potential duration bifurcation diagram, generated with the Shiferaw et al. model [54] in a one-dimensional cable. When pacing at a relatively slow rate, identical action potentials occur each time a stimulus

is applied (i.e., 1:1 behavior). However, increasing the pacing rate causes the action potential behavior to bifurcate, such that for every two stimuli, two different action potentials occur (i.e., 2:2 behavior).

The APD restitution curve is generally a monotonically increasing function as shown in Fig. 31.2. This reflects the fact that if a cell is allowed less time to recover before being excited, its action potential will be shorter. During constant pacing, a stable period 1 solution usually occurs, where each APD (and DI) is the same as the previous APD (or DI). Thus, for each stimulus input there is one APD; this is typically known as a 1:1 response.

In many cells, however, a critical stimulation rate exists at which a bifurcation to a qualitatively different behavior occurs [29, 43]. When paced faster than this critical rate, a stable period-2 behavior occurs, during which the action potential duration alternates on a beat-to-beat basis and returns to a given state after every two periods (i.e., after two action potentials) instead of after one, as shown in Fig. 31.3. That is, during alternans, there is a 2:2 response – two action potentials of different duration occur for every two periodic stimuli. The particular excitation rate at which the action potential activity in a given cell bifurcates to alternans is dependent upon the membrane currents and intracellular regulatory mechanisms operating in that cell.

Our interest in alternans resides in the role of alternans as a precursor, or even as a trigger event, for more complex and potentially fatal cardiac arrhythmias. The details of the implications of APD alternans for ventricular arrhythmias will be discussed in Section 31.3.3, while research toward controlling alternans is discussed in Section 31.5.

31.3 Cardiac Arrhythmias

The normal (sinus) rhythm of cardiac activation described in Section 31.2 can be disrupted in many ways leading to very different types of cardiac arrhythmias. Arrhythmias may range from benign, to debilitating, to fatal. Some occur

as a consequence of chronic heart disease while others may be triggered in healthy hearts.

Two of the most commonly occurring and potentially lethal cardiac arrhythmias are ventricular tachycardia and ventricular fibrillation. Ventricular fibrillation is thought to be the arrhythmia typically underlying sudden cardiac death. Mainly because of their severity, much of the current research on arrhythmia control has focused on these arrhythmias.

Ventricular tachycardia and ventricular fibrillation are both so-called reentrant arrhythmias. In this section, we briefly describe these arrhythmias and discuss how they may arise.

31.3.1

Reentry

Reentrant arrhythmias occur when tissue is repeatedly activated by an activation wave that again and again reenters the same anatomical region and reactivates it. A simple model of reentry is the closed ring, shown in Fig. 31.4A, where the activation wavefront rotates around an anatomical obstacle (e.g., scar tissue or a valve). This type of reentry can be identified by the following characteristics: (1) an area of unidirectional conduction block must exist at the time of reentry initiation, causing the activation wavefront to move in one direction only around the ring; (2) the activation wavefront must move around an anatomically distinct pathway, returning to its point of origin and then following the same path again; and (3) interruption of the reentrant circuit at any point along its path should terminate the circus movement. For a given closed circuit to form a reentrant ring, the rotation time around the ring must be longer than the recovery period of all segments of the circuit.

In the absence of an anatomical obstacle, it is still possible for circus movement reentry to occur. In such a situation, the activation wavefront rotates around a region that may be anatomically continuous, but which is functionally discontinuous. Such a situation occurs in the leading-circle/figure-of-eight/

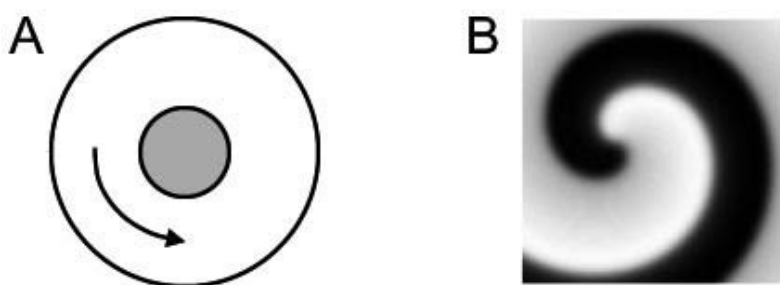


Fig. 31.4 Schematic illustration of anatomical (A) and functional (B) reentry. In anatomical reentry a wave cycles around an anatomical obstacle, while functional reentry may occur in completely homogeneous tissue, when a functional discontinuity at the tip of a spiral wave serves as a pivot point. Spiral waves may also become anchored to obstacles, causing anatomical reentry.

spiral-wave models of reentrant arrhythmias [4], where a functional discontinuity (instead of an anatomical discontinuity) serves as a pivot point about which the activation wave rotates. The functional discontinuity can be created by a region of depressed excitability (from residual or sustained refractoriness), or, in the case of spiral waves (Fig. 31.4(B)), by the high degree of curvature of the activation wavefront at the pivot point [5].

31.3.2

Ventricular Tachyarrhythmias

Some ventricular tachycardias are associated with the existence of a single reentrant circuit. This rhythm may terminate spontaneously if, for example, the wavefront catches up to the tail, or if the reentrant activity is disrupted by a different wavefront, for example one originating from the SA node. Alternatively, the reentrant circuit may destabilize and the reentrant wave may break up into multiple waves that can propagate into different regions of the ventricles. This can lead to the highly disorganized state of ventricular fibrillation.

While ventricular tachycardia can lead to excessively rapid contraction, potentially causing a reduction in the efficiency with which blood is pumped throughout the body, ventricular fibrillation leads to uncoordinated contraction and a drastic reduction in blood flow around the body. Unless defibrillation restores normal ventricular activation patterns within a few minutes of the onset of the arrhythmia, ventricular fibrillation invariably leads to death.

31.3.3

Alternans as an Arrhythmia Trigger

Initiation of ventricular tachyarrhythmias is sometimes preceded by the occurrence of alternans. As outlined below, it is possible that alternans actually causes the onset of some arrhythmias.

In tissue, alternans may occur in different spatial patterns. One type of pattern is spatially concordant alternans, where the tissue everywhere exhibits a long action potential on one beat and everywhere a short action potential on the next beat. A second type of pattern is spatially discordant alternans, where (at least) one region is out of phase and exhibits a long action potential, while for the same beat another region exhibits a short action potential. Discordant alternans may arise even in spatially homogeneous tissue, due to dynamically induced spatial variations in the conduction velocity of the propagating waves.

Discordant alternans may initiate arrhythmias through unidirectional block, which can occur when a propagating wave enters a region where a long action potential has left the tissue with too little recovery time for the wave to propagate further, while a neighboring region having had an action potential of shorter duration allows for propagation. Evidence of causality between alternans and the onset of arrhythmias has been demonstrated in experiments [10, 24, 46] and in computer simulations [24, 38, 48].

31.4

Current Treatment of Arrhythmias

Cardiac arrhythmias are currently treated using one or more of the following strategies: pharmacological treatment, implantable devices, and ablation therapy. For more details on the treatments described below, refer to [37].

31.4.1

Pharmacological Treatment

Despite a number of large clinical trials investigating the influence of an array of putative antiarrhythmic drugs, to date, only one class of drugs, β -blockers, which inhibit sympathetic nervous stimulation, have been demonstrated to be effective in preventing sudden cardiac death [33]. Some agents that block ion-specific channels have been tested in clinical trials, but they have either been proven ineffective or, worse, they have paradoxically increased mortality [59, 60]. These findings have made safety a key consideration in the development of new drugs, cardiac and otherwise, to the point where all new drugs are evaluated for inducing prolongation of the QT interval on the electrocardiogram, the most common adverse side effect. Recently, ACE inhibitors, which have long been the gold standard in treatment of high blood pressure, have shown promising results in terms of reducing the risk of sudden cardiac death [20].

Because of the limitations of current antiarrhythmic drugs, a recent book on the pharmacological treatment of cardiac arrhythmias states that the first principle of treating arrhythmias is to “avoid using antiarrhythmic drugs whenever possible” [22]. Consistent with this view, there has been an ongoing shift in emphasis in the therapies for ventricular arrhythmias, from pharmacological to nonpharmacological approaches [56]. Implantable devices (such as implantable cardioverter defibrillators) and ablative therapies have now become the therapies of choice for many patients, reflecting the demonstrated efficacy of these approaches and the recognition of the inherent risks, particularly the proarrhythmic effects, associated with long-term antiarrhythmic drug use [51].

31.4.2

Implantable Cardioverter Defibrillators

While pharmacological treatment is sometimes useful for preventing tachyarrhythmias from occurring, implantable cardioverter defibrillators (ICDs) attempt to terminate tachyarrhythmias once they have initiated. In 2003, an estimated 150,000 defibrillators were implanted in patients in the United States, with that number expected to increase in the coming years [35].

The first task of the ICD is to detect tachyarrhythmias. This is accomplished by the microprocessor, which continuously analyzes the recorded signals to determine whether an arrhythmia is occurring. Because mistakes can be deadly (in the case of a missed arrhythmia) or painful (in the case of a nonpathological

rhythm identified as a ventricular arrhythmia such that a defibrillation shock is delivered to a conscious patient), devices typically employ a combination of complementary detection techniques which examine such variables as rate, morphology, onset, regularity, and relationship of atrial and ventricular activity. Extensive research into such electrocardiogram processing techniques has greatly improved the accuracy of detection algorithms.

Once a tachyarrhythmia is detected, a suitable therapy must be delivered. The first therapeutic modality is antitachycardia pacing, which applies one or more series of suprathreshold (but not large enough to be perceptible to the patient) stimuli. Antitachycardia pacing is typically attempted for ventricular tachyarrhythmias exhibiting rates of up to 200–220 beats/minute [42] and aims to force a stimulated wave into the reentrant circuit to collide with and extinguish the reentrant wave. It was recently reported that antitachycardia pacing was effective in terminating 90% of ventricular tachyarrhythmias on which it was attempted [52].

High-energy defibrillation shocks are delivered when antitachycardia pacing fails or as primary therapy when arrhythmias such as ventricular fibrillation are detected. The defibrillation discharge typically occurs along multiple vectors, such as one defibrillation coil to another, or one defibrillation coil to the pulse generator. This approach helps ensure adequate “coverage” of the fibrillating myocardium.

Although ICDs are highly effective devices, they do have certain limitations. Up to one-third of defibrillation shocks are given at inappropriate times [6, 19, 57]. These inappropriate shocks can cause intense pain and chronic anxiety. In addition, the large shocks drain the battery of the ICD, thereby shortening the device lifetime. Improved detection algorithms may prevent unnecessary shocks from being delivered, but from the standpoint of survival, the results of a false-positive detection are likely to be far less detrimental than the results of a false-negative detection [34].

31.4.3

Ablation Therapy

Some arrhythmias can arise from a localized, abnormal region of cardiac tissue. In addition, reentrant tachyarrhythmias may require one or more critical anatomical regions of abnormal excitability or propagation to be sustained. Recognizing this fact, ablation of viable tissue in such a region can be used to treat some arrhythmias. With this technique, radiofrequency energy destroys tissue by resistive heating that creates a nonviable lesion.

Perhaps the most difficult aspect of radiofrequency catheter ablation is localization of the correct ablation site. Furthermore, especially for reentrant tachyarrhythmias, it is often necessary to reposition the catheter multiple times near the site to achieve an adequate scar, as radiofrequency lesions are relatively small in diameter and depth. The lack of depth also makes radiofrequency ablation ineffective in those situations where the abnormal region is situated well within the myocardium. This is more often the case in the ventricles than in

the atria, because of the thickness of the ventricular wall. In contrast, the much thinner atrial wall makes radiofrequency ablation useful for treatment of many atrial arrhythmias.

31.5 Alternans Control

While the ICD has been highly successful in saving lives, it has some inherent disadvantages, as discussed above. Antitachycardia pacing sometimes fails, in which case the ICD reverts to its high-energy defibrillation mode. Furthermore, defibrillation is not always successful. Hence, a preferable strategy would be a device that prevents tachyarrhythmias from occurring in the first place, by recognizing and stopping precursor events using small amplitude electrical stimuli. Control of APD alternans is one such strategy currently under investigation.

31.5.1

Controlling Cellular Alternans

Recent research has suggested that control algorithms targeted at cardiac alternans could potentially lead to an improvement in the therapeutic efficacy of implantable devices such as ICDs.

Most of this work is based on model independent, adaptive control algorithms, e.g., delayed-feedback control (DFC). In this method, which is based on the Ott-Grebogi-Yorke (OGY) [44] technique for chaos control, small perturbations are applied to the timing of the next excitation in an attempt to force the state of the system toward the (unstable) period-1 fixed point. Unlike chaos control techniques, DFC algorithms do not require a learning stage (i.e., learning the dynamics in the neighborhood of the unstable period-1 solution). This is important, because during alternans, the dynamics evolve far from the period-1 dynamics (unless the alternans amplitude is very small). Delayed-feedback control (DFC) algorithms typically require (i) knowledge of the state of the system for a very short time history, and (ii) a basic understanding of the system dynamics to ensure that the control perturbations are of the proper magnitude and polarity. These two elements allow the periodic rhythm to be stabilized by repeated adjustment of the stimulation time.

Let BCL (basic cycle length) be the time interval between two stimulations. A typical DFC algorithm for alternans control is:

$$\text{BCL}_{n+1} = \begin{cases} \text{BCL}^* & \text{for } \Delta\text{BCL}_{n+1} > 0, \\ \text{BCL}^* + \Delta\text{BCL}_{n+1} & \text{for } \Delta\text{BCL}_{n+1} \leq 0, \end{cases} \quad (31.1)$$

with

$$\Delta\text{BCL}_{n+1} = \frac{\gamma}{2} (\text{APD}_{n+1} - \text{APD}_n), \quad (31.2)$$

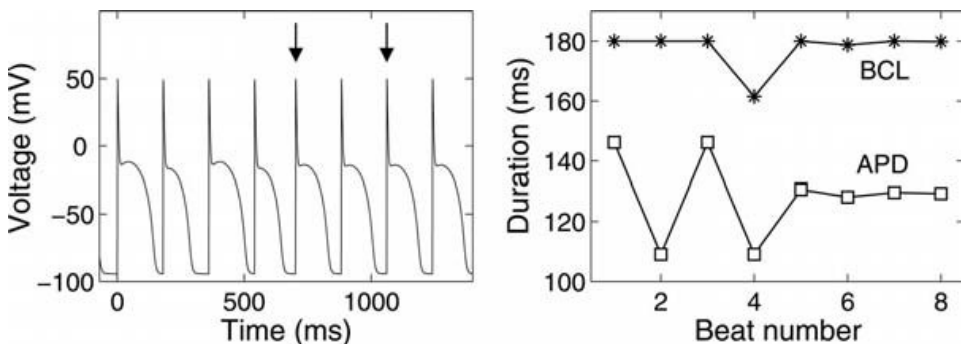


Fig. 31.5 Action potential duration (APD) alternans control in the Fox et al. model of the canine ventricular action potential [23]. Alternans is induced by rapid pacing at a basic cycle length (BCL) of 180 ms. Delayed-feedback control (DFC) is turned on after the first four action potentials. DFC works by

shortening the BCL of the cycles with short APDs by delivering premature stimuli (arrows), thereby shortening the recovery interval and hence also shortening the subsequent APD. The value of the feedback gain (γ) is 1.0.

where γ is the feedback gain and BCL^* is the nominal BCL. The restriction that a perturbation is only given to shorten, and not delay, the intrinsic rhythm reflects the fact that, in the heart, it is often not possible to delay the excitation: it will occur naturally without stimulation. Thus, this algorithm is said to be restricted. Both unrestricted DFC algorithms (which allow both lengthening and shortening of the BCL during control) and restricted DFC algorithms have been applied to cardiac rhythm disturbances.

An example of alternans control in a mathematical model is shown in Fig. 31.5. Essentially, the restricted algorithm works by shortening the long DI by giving a premature stimulation. This in turn shortens the long APD due to restitution, as described in Section 31.2.1. Eventually, the unstable period-1 solution is stabilized and action potentials of constant duration are established. The rate of convergence is controlled by the feedback gain.

DFC has been used experimentally to control APD alternans in small pieces (i.e., sufficiently small to be point like) of bullfrog hearts [30]. Provided that the feedback gain was within an appropriate range of values, the period-2 alternans rhythm was successfully controlled to the underlying unstable period-1 rhythm.

DFC algorithms have also been used to control a related type of alternans (atrioventricular (AV) nodal conduction alternans; a beat-to-beat alternation in the conduction time through the AV node) [12, 16, 32]. To date, AV node alternans control is the only alternans control study performed on human subjects [16].

31.5.2

Control of Alternans in Tissue

While APD alternans could be successfully eliminated in a system that does not have spatiotemporally varying repolarization and wave-propagation dynamics (the frog sections in [30] were small enough that there were no apparent spatial

variation in dynamics), research on how to control APD alternans in spatially extended systems (i.e., tissue rather than cells) is still in its infancy.

The utility of adaptive control algorithms for terminating potentially dangerous rhythms such as APD alternans will only become obvious once further research is conducted into the effectiveness of such algorithms in controlling arrhythmias spatially as well as temporally. Initial analytical work as well as computer simulations of one-dimensional fibers suggest that only in the case of spatially uniform APD alternans can alternans be terminated along the whole fiber. In cases where concordant alternans show variation in space, as well as in the more extreme cases of spatially discordant alternans, eliminating APD alternans at one site will result in APD alternans being eliminated only up to a short distance away from this stimulation site [21, 49].

Recent experiments in canine Purkinje fibers qualitatively confirm these predictions [15]. Interestingly, these experiments also showed that APD alternans of relatively small amplitude could be controlled over larger distances. Thus if one can detect the early onset of small amplitude APD alternans, control should be more easily achieved. In addition, these experiments showed that discordant alternans could be converted to concordant alternans. Since discordant alternans pose a larger risk of inducing tachyarrhythmias than concordant alternans, this finding is quite intriguing.

To date, there have been no experimental studies of the actual distance over which DFC control algorithms suppress alternans in ventricular tissue. If the distance is short, such that multiple stimulation sites are necessary in order to simultaneously suppress APD alternans in different regions of the heart, a cardiac device that fits snugly around the ventricles, perhaps similar to one (the CorCap™ Cardiac Support Device, by Acorn Cardiovascular) that is now in clinical trials as a therapy for heart failure [45] could potentially be developed.

Another concern regarding APD alternans control in ventricular tissue is ionic heterogeneity. There are intrinsic differences in ionic properties, such as ion channel densities, in different regions of the ventricles, e.g., across the ventricular wall, between the apex and the base, between the left and the right ventricle, and between the posterior and the septal wall of the left ventricle [62]. At present, it is not known how this may affect the ability to control APD alternans in the ventricles. One thing to keep in mind, though, is that from a clinical point of view it would be beneficial to simply turn discordant alternans into concordant alternans, or to reduce the alternans amplitude. Complete elimination of alternans everywhere in the tissue may not be necessary in order to significantly reduce the risk of tachyarrhythmias.

31.5.3

Limitations of the DFC Algorithm in Alternans Control

In addition to the afore-mentioned complications in tissue, the DFC algorithm has certain more fundamental limitations. When DFC algorithms are used to control periodic rhythms, rapid convergence to the period-1 rhythm is achiev-

able only if the feedback gain (γ) is at or near its optimal value. The optimal value of the feedback constant is a function of the degree of instability of the fixed point [27]. Because estimation of the instability of the fixed point requires that the system state point visit the neighborhood of the fixed point, determination of the optimal feedback constant value during periodic rhythms is difficult. (Algorithms that utilize external perturbations to explore the neighborhood of the period-1 fixed point can sometimes be used to estimate this optimal value [11].) Additionally, not only does convergence rate decrease with increasing distance from the optimal proportionality constant value, but control fails when the proportionality constant lies outside an acceptable range of values. While algorithms that iteratively adapt the feedback constant to achieve control do exist [14, 31], such algorithms can be sensitive to the noise and nonstationarities that are typically present in experiments.

31.5.4

Adaptive DI Control

Although the DFC algorithms have proved effective for controlling APD alternans, an alternative approach that is based solely on cardiac electrophysiological principles has also been developed [36, 47]. This cardiac-specific control algorithm exploits the restitution properties of cardiac tissue to control both periodic and aperiodic rhythm disturbances to a period-1 rhythm, and does not require the dynamics of the system to be learned.

Consider the APD alternans occurring at a basic cycle length BCL^* shown in Fig. 31.6. The AP alternates between points A and B on a beat-to-beat basis. Because $APD_n + DI_n = BCL^*$, DI_n alternates as well. In DI control, alternans can be suppressed by perturbing BCL^* on a beat-to-beat basis such that DI_n is kept at a constant target value. Due to the functional dependence of APD_{n+1} on DI_n characterized by the restitution curve, stimulation such that consecutive DIs are identical causes each subsequent AP to converge to a constant repeating morphology.

Similarly to the feedback gain (γ) in the DFC algorithm, the adaptive DI control method makes progressively smaller perturbations to the cycle length. This adaptive DI (ADI) control technique involves selecting an initial target DI and then adjusting this value on a beat-to-beat basis until the sum of the target DI and subsequent APD is equal to the original basic cycle length BCL^* (i.e., $DI_n + APD_{n+1} = BCL^*$). The target DI is adaptively lengthened on a beat-to-beat basis according to the control rule

$$DI_{n+1} = a(BCL^* - BCL_n) + DI_n, \quad (31.3)$$

where a is a constant between 0 and 1 that controls the rate at which DI_n changes. During ADI control, the difference between the present cycle length (BCL_n) and the original cycle length (BCL^*) is therefore reduced until $BCL_n = BCL^*$, and the period-1 rhythm will have been established at the origi-

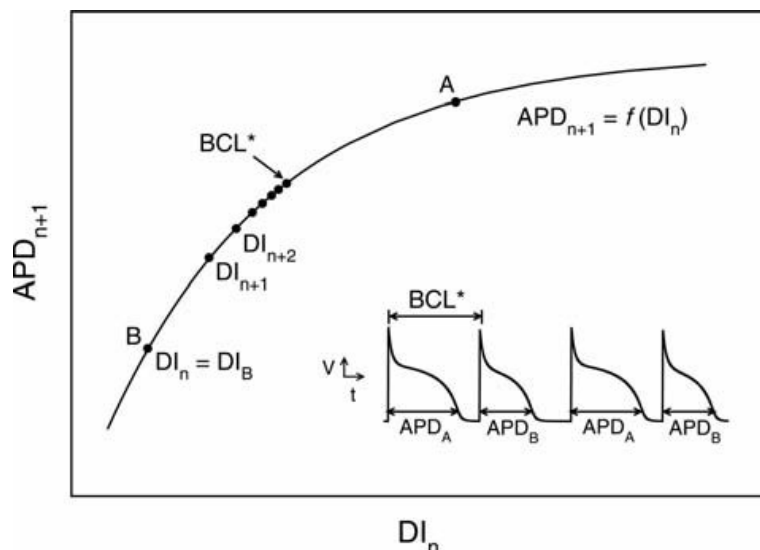


Fig. 31.6 Schematic representation of the DI and adaptive DI (ADI) control schemes. APD initially alternates between points A and B on the restitution curve during stimulation at the basic cycle length BCL^* . The inset illustrates the voltage profile of this alternans rhythm prior to the onset of control. Initiation of DI control when $DI_n = DI_B$ makes every subsequent DI equal to DI_B ,

and hence each subsequent APD will be equal to APD_B . Alternatively, ADI control may also be initiated with the target DI set to DI_B , as $DI_B + APD_B < BCL^*$. The target DI is then lengthened according to the control rule of Eq. (31.3), such that each successive APD climbs up the restitution curve until the cycle length ($DI_n + APD_{n+1}$) is again equal to BCL^* .

nal cycle length BCL^* . This period-1 rhythm is the same as the unstable period-1 fixed point obtained by existing DFC algorithms. However, as Eq. (31.3) indicates, the ADI control approach is fundamentally different from DFC.

Adaptive DI control has been successful in obtaining control in numerical simulations [36]. However, there are certain limitations to the method. One concern is that DI control is based on the assumption that the AP dynamics is captured by a one-dimensional map. Recent studies have shown that intracellular calcium dynamics contributes to the development of alternans, adding to the complexity of the problem. Indeed, APD alternans may occur even when DI is fixed [17, 63]. Still, the extent to which the restitution assumption fails is under investigation and is likely to vary between cell types and species.

31.6 Control of Ventricular Tachyarrhythmias

Due to its inherent disorganization, ventricular fibrillation is much more difficult to tame with control algorithms than ventricular tachycardia or alternans. Both because antitachycardia pacing (and perhaps alternans control in future devices) sometimes fails, and because fibrillation sometimes occurs directly from sinus rhythm with no apparent warning or trigger, it is critically important

for devices to be able to defibrillate the heart. Much of the work in defibrillation research focuses on reducing the energy requirements for successful defibrillation. Smaller shocks both drain the device battery less and are less painful for the patient.

Since the dynamics of ventricular fibrillation are aperiodic, and perhaps chaotic, one way of reducing the necessary shock strength may be to apply chaos control methods. In pioneering studies, Garfinkel et al. applied OGY-type control algorithms to rabbit ventricle preparations exhibiting aperiodic, possibly chaotic, dynamics [26]. The rhythm was controlled, but to a period-3 rhythm, rather than the desired period-1 rhythm. A later mathematical study demonstrated that such control results may have resulted from mis-estimation of the period-1 rhythm [13]. In another study of aperiodic dynamics, a cardiac-specific control algorithm applied to a simulated chaotic action potential duration time series was successful in controlling the unstable period-1 rhythm at certain excitation rates [61]. Clinical realizations of these defibrillation methods are still speculative, but would almost certainly involve multiple sites for recording and stimulation.

In the remainder of this section, we will focus on termination of ventricular tachycardia. Please refer to the chapter by S. Sinha and S. Sridhar in this volume for defibrillation approaches.

31.6.1

Suppression of Spiral Waves

Because spiral waves are associated with ventricular tachycardia, several methods have been proposed for terminating spiral waves. Some of the methods are aimed at driving the spiral wave out of the tissue by local external forcing [8, 39, 41]. In the heart, the spiral would have to be forced into some nonconductive region.

Other methods have been based on feedback control. In one such simulation study, small stimuli delivered during the repolarization phase of the action potential were effective in preventing a spiral wave with alternans dynamics from breaking up into fibrillatory-like activity [49]. In other simulations, alternans-induced spiral breakup has been prevented by applying a single, well-timed stimulus during the repolarizing phase using a special algorithm based on the eigenmodes of the model equations [3].

The extent to which some of these methods for spiral wave control are feasible as therapeutic strategies remains unclear and requires further study.

31.6.2

Antitachycardia Pacing

As described in Section 31.4.2, the antitachycardia pacing modality of the ICD works quite well in many cases. The ICD is usually programmed to give either a burst of 8–10 electrical stimuli of constant frequency (faster than the reen-

trant rhythm), or a train of 8–10 stimuli with increasing frequency. Since the stimulating electrode is not necessarily situated inside the reentrant loop, it is thought that the earlier stimuli “peel back” refractoriness to allow the subsequent stimuli to enter the reentrant loop and terminate the tachycardia. However, there is no known clear physical mechanism explaining how antitachycardia pacing works in the heart.

A simple model of ventricular tachycardia is a reentrant wave traveling around a one-dimensional ring. In this model, where the stimulus site is necessarily in the reentrant circuit, it is well known how even a single stimulus may terminate the reentrant dynamics. Consider the situation in Fig. 31.7(A), where reentrant wave is traveling around the ring. If the stimulus is given too soon after the passing of the previous wave when the tissue at the stimulus site is still refractory, the stimulus cannot induce a full action potential and has only very little effect on the reentrant wave (Fig. 31.7(A)). On the other hand, if the stimulus is given after some delay since the passing of the previous wave, a pair of waves are generated, traveling in opposite directions away from the stimulus site (Fig. 31.7(C)). The wave traveling in the retrograde direction to the original reentrant wave will collide with and annihilate the original wave. However, the wave traveling in the anterograde direction will continue to circulate, replacing

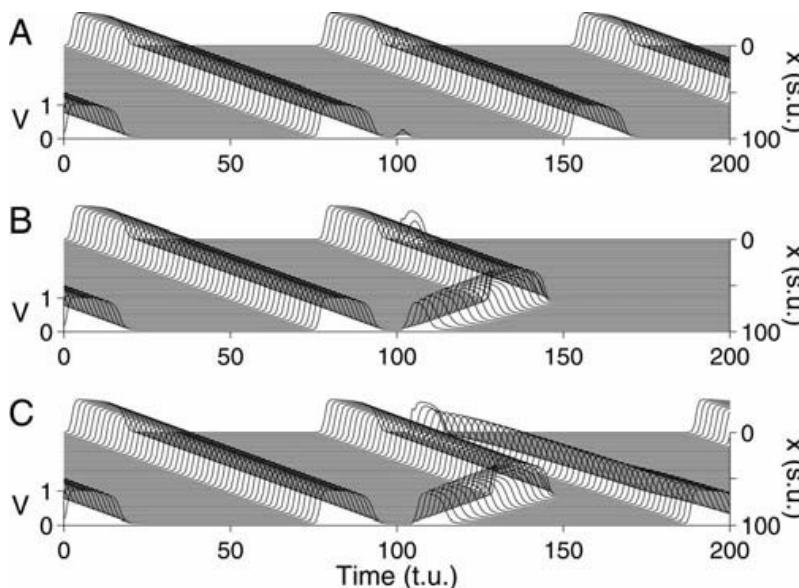


Fig. 31.7 Pacing-induced termination of reentry in a one-dimensional loop of length 100 space units (s.u.). The figure was generated using the Aliev-Panfilov version of the FitzHugh-Nagumo model [2]. The timing of the stimulus (t_s) is varied between the three panels: $t_s = 99$ time units (t.u.) (A), $t_s = 101$ t.u. (B), and $t_s = 104$ t.u. (C). When the stimulus is given too early, it does not generate new waves (A). If the stimulus is given

later, two waves are induced traveling in opposite directions on the ring. One wave terminates the original reentry, but the other wave persists, such that a reentry remains (C). In contrast, if the stimulus is given within the so-called vulnerable window, the stimulus-induced wave is unidirectionally blocked and propagates in the retrograde direction only, where it will terminate the original reentry (B).

the original wave. Hence, termination was not successful. Based on continuity arguments, however, there must be an intermediate timing of the stimulus for which the reentry is terminated [28]. This happens when a well-timed stimulus causes the induced wave to be blocked unidirectionally and travel in the retrograde direction only, while the tissue in the anterograde direction is still refractory and does not allow for propagation. The wave induced by the stimulus collides with and terminates the original reentrant wave and termination is successful (Fig. 31.7(B)).

There are several problems in terms of extrapolating this simple model to the heart. The stimulus has to fall into a narrow time interval (typically a few milliseconds), called the vulnerable window, in order for termination to be successful. In addition, the vulnerable window effectively disappears when the stimulus site is located at some distance away from the ring [55]. Finally, the heart is three dimensional, which gives additional complexities.

Still, promising work is being done in this area. Simulation studies have shown how using a pair, rather than single, stimuli increases the vulnerable window from a few milliseconds to tens of milliseconds by mechanisms other than unidirectional block [18]. Other simulation studies have shown how burst pacing with > 12 stimuli may lead to termination even when the stimulus site is located at some distance from the reentrant loop [9].

Further studies are needed to give a clear physical understanding of the mechanisms of antitachycardia pacing. It is entirely possible that such explanations will point toward new methods for improving therapy.

31.6.3

Unpinning Spiral Waves

Spiral waves associated with ventricular tachycardia are often anchored or pinned to anatomical obstacles in the heart. When pinned, the spiral wave can be very stable and would be expected to be difficult to force out of the heart using the methods described in Section 31.6.1.

Simulations studies have shown that it is possible to unpin a spiral from a small obstacle using burst pacing [25]. However, for larger obstacles where the “force of attraction” between the spiral core and the obstacle is greater, it may be necessary to give a stimulus at the obstacle to unpin the spiral. In clinical situations, however, the stimulus electrode is most likely not situated exactly at the obstacle.

One potential way of circumventing this problem is the following: when an electrical field is applied to tissue with an inexcitable obstacle, a so-called virtual electrode is formed, where a region of tissue neighboring one side of the obstacle is depolarized, while a region of tissue neighboring the opposite side is hyperpolarized. If the timing is right, and the depolarization is of sufficient amplitude, a new wave is generated at the obstacle and thus inside the reentrant circuit, and the spiral is unpinned [58]. This method has been tested in preparations from rabbit hearts, where it may be even more effective than classic

antitachycardia pacing [50]. One possible limitation of this method is that the spiral may repin to the same obstacle or a different obstacle.

31.7 Conclusions and Prospects

The concept of using nonlinear dynamical control methods to control aperiodic electrical activity in animal cardiac tissue preparations was shown to be effective a decade and a half ago [26]. However, successful application of such approaches to terminate ventricular fibrillation in human hearts is still lacking. Given that there may be many spiral waves present in the ventricles during fibrillation, control methods based on application of local stimuli would likely require multiple recording and stimulation sites. While this is less practical than having a single site, it may still be possible to implement in implantable devices. Another difficulty in controlling ventricular fibrillation *in vivo* lies in the fact that cardiac tissue rapidly becomes ischemic during ventricular fibrillation due to lack of pumping of blood. A control algorithm would either have to rapidly terminate ventricular fibrillation, or be able to integrate the nonstationary dynamics.

Because of difficulties in controlling ventricular fibrillation, we believe that other strategies may lead to faster improvement in preventing sudden cardiac death. One approach is to attempt controlling arrhythmia precursor events such as electrical alternans. However, more research is necessary in order to determine the tissue volume over which a single electrode can control alternans. As mentioned, in contrast to fibrillation, which must be terminated in order to prevent a patient from dying, alternans need not necessarily be annihilated; a decrease in the alternans amplitude may reduce the risk of onset of ventricular tachyarrhythmias.

Another strategy to prevent sudden cardiac death is to improve antitachycardia pacing. The first step in this direction could be to determine the exact mechanisms of success versus failure of antitachycardia pacing. Utilizing such understanding might lead to the design of more effective pacing algorithms.

Because cardiac arrhythmias are characterized by complex nonlinear dynamics, tools and approaches from mathematics and physics have made, and are likely to continue making, important impacts on mechanistic understanding and therapy innovations.